

1
2
3
4 Description and initial simulation of a dynamic bi-directional air-
5 surface exchange model for mercury in CMAQ
6

7
8 Jesse O. Bash¹

9 ¹U.S. Environmental Protection Agency
10 National Exposure Research Laboratory
11 Research Triangle Park, NC 27711
12

13
14
15
16 **Abstract:**

17 [1] Emissions of elemental mercury (Hg^0) from natural processes are estimated to
18 be as large as or larger than anthropogenic emissions and thus represent a critical process
19 which must be accurately described in the modeling of the transport and fate of mercury.
20 Recent ecosystem scale measurements indicate that a fraction of recently deposited
21 mercury is recycled back into the atmosphere quickly, and that an atmospheric
22 compensation point exists at background ambient concentrations. Modeled Hg^0 emissions
23 from natural sources are typically uncoupled from dry deposition estimates and
24 unconstrained by air-biosphere gradient processes. A module has been developed for the
25 Community Multiscale Air Quality (CMAQ) model to parameterize concentration-
26 dependent processes of bi-directional mercury exchange. The Hg^0 air-surface exchange
27 was modeled as a function of a dynamic compensation point. The compensation point is
28 modeled as a function of sources and sinks of Hg^0 in vegetation and soil media using

1 partitioning coefficients. A box model simulation was run for five months and a CMAQ
2 simulation with bi-directional (BIDI) and without bi-directional (BASE) mercury
3 exchange was run for the month of July 2002. The BASE case modeling scenario
4 estimated that 8.5% of the total mercury deposited to terrestrial systems and 47.8% of the
5 total mercury deposition to aquatic systems was re-emitted as Hg^0 , while the re-emission
6 ratios were 70.4% and 52.5% in the base case. The BIDI case was in better agreement
7 with recent estimates of mercury cycling using stable isotopic mass balance experiments.
8

1 **1. Introduction**

2 [2] Atmospheric mercury exists predominantly in the elemental form, Hg^0 , which
3 has a relatively long atmospheric lifetime of 0.5 to 1.5 years [*Lindberg et al.*, 2007].
4 However once oxidized into reactive divalent, Hg^{2+} , or particulate, PHg, species it can be
5 rapidly removed from the atmosphere through wet and dry deposition pathways
6 [*Lindberg et al.*, 2007]. The formation of Hg^{2+} and PHg can be rapid under the right
7 conditions [*Weiss-Penzias et al.*, 2003] and may be better parameterized regionally than
8 globally [*Hedgecock and Pirrone*, 2004]. The long atmospheric lifetime and emission of
9 Hg^0 from natural processes can lead to transport and deposition to sensitive ecosystems
10 located far from anthropogenic sources [*U.S. EPA*, 1997; *Fitzgerald et al.*, 1998].

11 [3] Anthropogenic activities have increased the global mercury pool actively
12 cycling between the atmosphere and biosphere by approximately a factor of three
13 [*Lindberg et al.*, 2007]. Recently, a link between mercury deposition and methylation in
14 water bodies has been established [*Hammerschmidt and Fitzgerald*, 2006; *Orihel et*
15 *al.*, 2007] and wildlife has been shown to be adversely effected by the bioaccumulation of
16 methylmercury through the food web [*Wolfe et al.*, 1998]. Segments of the human
17 population vulnerable to the impacts of mercury contamination have been adversely
18 affected primarily through the consumption of fish with high levels of methylmercury
19 [*Sunderland*, 2007]. Accurate estimates of mercury loading to ecosystems are needed to
20 characterize the risk posed by methylmercury production in sensitive ecosystems that can
21 adversely affect human and ecosystem health.

22 [4] Atmospheric wet and dry deposition are the primary source of mercury
23 contamination in most sensitive ecosystems. Once deposited, divalent forms of mercury

1 can be reduced to the zero valence state evade back to the atmosphere or become
2 methylated into toxic methylmercury compounds under anoxic conditions [*Lindberg et*
3 *al.*, 2007]. *Xin et al.* [2007] observed a hysteresis in the mercury flux from soils under
4 decreasing ambient concentrations indicating that deposition to soil surfaces is reversible
5 and dependent on previous fluxes. In addition, atmosphere-vegetation compensation
6 points have been documented at background ambient concentrations using dynamic
7 chamber techniques [*Graydon et al.*, 2006; *Poissant et al.*, 2008] and
8 micrometeorological techniques [*Bash and Miller*, 2009]. These processes can be
9 modeled using a dynamic compensation point model, where the compensation point is
10 defined as the ambient concentration where the net air-surface flux is zero [*Flecharde et*
11 *al.*, 1999]. Ambient concentrations greater than the compensation point will lead to
12 atmospheric deposition and while concentrations less than the compensation point will
13 lead to evasion from the surface.

14 [5] Recent whole ecosystem mercury loading studies using stable isotopes have
15 elucidated the retention and transport of deposited mercury. Stable mercury isotopes were
16 added as HgCl_2 in an aqueous solution to the remote experimental lakes area (ELA) in
17 northwestern Ontario to increase the mercury loading to levels experienced by more
18 polluted areas, 120% of the background wet deposition loading at ELA, and to trace the
19 biogeochemical cycling of mercury through a forested watershed, wetlands, and in
20 surface waters [*Hintelmann et al.*, 2002]. Stable Hg isotopes were applied to an upland
21 forest catchment, wetlands, and the lake surface. Fluxes were determined by applying a
22 mass balance method to soil, vegetation, runoff, and water samples [*Hintelmann et al.*,
23 2002]. These studies have shown that recently deposited mercury is more readily

1 transported and methylated [*Hintelmann et al.*, 2002; *Harris et al.*, 2007] and that the
2 fraction of deposited mercury that is re-emitted varies with land cover type [*Graydon et*
3 *al.*, 2008, *Harris et al.*, 2007]. In a summary of the studies *Harris et al.* [2007] estimated
4 that approximately 25-30% of the stable isotopes added to the upland and watershed
5 catchment and 45% added directly to the lake over three years were lost to evasion to the
6 atmosphere. Additionally and independent examination of the photochemical reduction of
7 mass dependent and independent fractionation of mercury isotope has been used to
8 estimate that $68.8 \pm 8\%$ to $25 \pm 8\%$ of surface water mercury was volatilized to the
9 atmosphere limiting the pool available for methylation and bioaccumulation [*Bergquist*
10 *and Blum*, 2007]. Air quality models must capture the bi-directional nature of the air-
11 biosphere exchange of mercury in order to provide accurate estimate the mercury loading
12 to sensitive ecosystems.

13 [6] Mercury emissions from natural processes are believed to range from
14 approximately 40% to 70% of the total mercury loading to the atmosphere [*Shetty et al.*,
15 2008; *Lindberg et al.*, 2007]. The parameterization of mercury evasion from natural
16 processes has been an active area of research [*Lindberg et al.*, 2007]. These emissions
17 from have been parameterized as an *a priori* as a global value constrained by estimates of
18 the biogeochemical cycle [*Seigneur et al.*, 2001; 2004], as a fraction of the total mercury
19 wet and dry deposition field [*Selin et al.*, 2008], as an empirical soil evasion processes
20 and as a function of evapotranspiration [*Shetty et al.*, 2008; *Gbor et al.*, 2006; *Bash et al.*,
21 2004; *Xu et al.*, 1999], and as a stochastic function of land cover type and meteorological
22 variables [*Lin et al.*, 2005]. Two-film air water exchange models have been used to
23 estimate Hg^0 evasion from water [*Shetty et al.* 2008; *Bash et al.* 2004] and a bi-

1 directional coupled air-sea exchange model for mercury was developed for GEOS-Chem
2 [*Strode et al.*, 2007], but a mechanistic bi-directional exchange model describing air-
3 terrestrial exchange has not yet been implemented.

4 [7] Specifying the mercury emissions as an *a priori* function of an annual estimate
5 of the mercury geochemical cycle [*Seigneur et al.*, 2001; 2004] or an instantaneous
6 deposition field [*Selin et al.*, 2008] leaves the emission field unconstrained by physical
7 transportation processes and assumes that both the earth's surface is an infinite sink for
8 deposition and the atmosphere is an infinite sink for emissions. Constraining the natural
9 mercury evasion using a resistance model improves mercury transport and fate [*Gbor et*
10 *al.*, 2006], but still assumes that the earth's surface and atmosphere are infinite sinks for
11 mercury. *Strode et al.* [2007] coupled the atmospheric and oceanic pools of mercury
12 using a two-film resistance model, thus constraining the emissions and deposition fluxes
13 with the parameterized physical transport processes in the resistance model and air-
14 surface water concentration gradients. More recently *Selin et al.* [2008] modeled the air-
15 terrestrial cycling of mercury as the instantaneous re-emission of 20% of wet and dry
16 deposited Hg^{2+} . This technique effectively reduces the deposition velocity of Hg^{2+} by
17 20% and estimates large evasive pulses during precipitation events when atmospheric
18 stability may or may not be able to sustain such turbulent transportation processes. It
19 does not propose the reduction mechanism(s) and is not supported by recent
20 measurements that indicate environmental reduction processes responsible for mercury
21 evasion are not instantaneous but, rather, are in response to environmental stimuli
22 following the deposition event [*Xin et al.*, 2007].

1 [8] This study describes the development and preliminary simulations of a model
2 that couples an Eulerian chemical transport model with a compartmental non-steady state
3 soil-vegetation-air transport model. Published octanol-water partitioning coefficients and
4 oxidation and reduction rates for mercury species in water, soil, and vegetation are used
5 to describe the bi-directional exchange of the air-biosphere cycling of mercury. The
6 octanol-water partitioning coefficient is most often used to model the exchange of
7 organics with vegetation surfaces but is applicable to inorganic species [Trapp 2004] and
8 was the only available partitioning coefficient based on published measurements that
9 distinguishes between Hg^0 and Hg^{2+} species.

10 [9] The mercury bi-directional exchange model estimates air-biosphere exchange
11 as a function of an atmospheric compensation point, atmospheric mixing processes, and
12 air-biosphere partitioning processes. This model has been included as a research option in
13 the multipollutant version of the Community Multiscale Air Quality (CMAQ) version
14 4.7, a widely used multi-pollutant regional air quality model [Byun and Schere, 2006].
15 The standard CMAQ without bi-directional exchange uses off-line estimates of direct and
16 recycled emissions of elemental mercury following Bullock *et al.* [2008] and
17 conventional estimates of dry deposition, where the deposition velocity is modeled as a
18 function of atmospheric and surface resistances (Figure 1a).

19 [10] Resistance models for species that have the potential for re-emission should
20 be parameterized in a more fundamental physical, chemical, and biological descriptive
21 way than using the uni-directional dry deposition concept [Wesely and Hicks, 2000]. The
22 bi-directional exchange module still parameterizes the transport of material to and from
23 surface media using a resistance analogy. However, an atmospheric compensation point

1 is estimated and the net air-surface exchange is parameterized as a function of this
2 compensation point, the ambient concentration and the resistances to mass transfer
3 between and within the media following the framework of *Bash et al.* [2007] (Figure 1b).
4 Elemental mercury evasion and deposition processes are estimated simultaneously, and
5 mass conservation is applied to the foliar, soil and surface water concentrations,
6 constraining the emissions to the mass of mercury previously deposited and the initial
7 conditions. Bulk soil Hg^{2+} concentrations are assumed to be constant over the simulation
8 period of a regional model (~ 1 year) because the soil mercury pool is several orders of
9 magnitude larger than the atmospheric mercury pool [*Lindberg et al.*, 2007]. The
10 potential for evasion from terrestrial and water surfaces is modeled as a function of the
11 integrated net surface exchange, initial concentration, and the reduction/partitioning
12 schemes.

13 [11] The CMAQ model has been extensively evaluated against observations of
14 wet deposition and other regional air quality models that include mercury chemistry
15 [*Bullock et al.*, 2009; *Bullock et al.*, 2008; *Ryaboshapko et al.*, 2007a; *Ryaboshapko et*
16 *al.*, 2007b; *Bullock and Brehme*, 2002]. Therefore, the newly developed bi-directional
17 mercury exchange model for CMAQ will be described in detail and its results will be
18 compared to a one month CMAQ mercury simulations using mercury emissions from
19 natural processes estimated following earlier studies [*Bullock et al.*, 2009; *Bullock et al.*,
20 2008] as well as mercury deposition network (MDN) measurements [*Lindberg and*
21 *Vermette*, 1995; *Vermette et al.*, 1995]. In this study, surface exchange of Hg^0 is defined
22 as the net exchange, i.e. (emissions – dry deposition). Surface exchange in CMAQ 4.7
23 BASE case is defined as the difference between natural emissions field from the 2002

1 NEI emissions inventory (version 3) and the modeled dry deposition field. Bi-directional
2 CMAQ 4.7, the BIDI case, couples the dry deposition and natural emissions fields as
3 described in the methods thus estimating the net surface exchange of Hg^0 directly for
4 each time step.

5 **2. Methods**

6 *2.1 Model Configuration and Scenarios*

7 [12] CMAQ 4.7 Multi-pollutant was run on a 36 km x 36 km horizontal grid and
8 14 layer vertical structure from July 1st to August 1st 2002 with (BIDI scenario) and
9 without the bi-directional (BASE scenario) mercury exchange module. This simulation
10 used a non-hydrostatic terrain following pressure vertical coordinate system with a
11 vertical extent to the 100 mb (~14 km) level. The CB-05 chemical mechanism [*Sarwar et*
12 *al.*, 2008], efficient Euler backward interactive (EBI) solver [*Hertel et al.*, 1993] and
13 AERO5 aerosol modules [*Carlton et al.*, 2008; *Carlton et al.*, submitted] were used for
14 both cases. Boundary and initial conditions for both simulations were provided by
15 GEOS-Chem Hg [*Strode et al.*, 2007]. The mean GEOS-Chem Hg initial conditions for
16 Hg^0 , Hg^{2+} , and PHg were 1.28 ng m^{-3} , 32.45 pg m^{-3} , and 2.04 pg m^{-3} respectively. The
17 boundary conditions were updated on three hour intervals and ranged from 1.77 ng m^{-3} to
18 1.03 ng m^{-3} with the highest concentrations at the north western lateral boundary and the
19 lowest concentrations at the south eastern lateral boundary. The vertical profiles of the
20 lateral boundary conditions were similar to the GEOS-Chem Hg boundary conditions
21 used in the North American Mercury Model Intercomparison Study (NAMMIS) *Bullock*
22 *et al* [2008] with an approximate 50% decrease in Hg^0 and PHg concentrations from the
23 model surface layer to the modeled top layer and an increase in Hg^{2+} concentrations from

1 ~30 pg m⁻³ at the surface layer to ~300 pg m⁻³ to the top layer. The first seven days of the
2 simulation were used as a spin up and were not included in the analysis. The 2002
3 anthropogenic emissions were provided by the EPA National Emissions Inventory (NEI)
4 (<http://www.epa.gov/ttn/chief/net/critsummary.html>) and processed by the Sparse Matrix
5 Operation Kernel (SMOKE) model [Houyoux et al., 2000]. Meteorological fields were
6 provided by the Penn State/NCAR fifth-generation mesoscale model (MM5) [Grell et al.,
7 1994] with the P-X land surface scheme [Pleim and Xiu, 1995] processed for CMAQ
8 with the Meteorology-Chemistry Interface Processor (MCIP 3.3). Both model scenarios
9 used the in-line calculation of dry deposition velocity option in CMAQ 4.7. A five
10 month simulation of the bi-directional exchange model was run using BASE model
11 output for ambient Hg⁰ and Hg²⁺ concentrations and MM5 meteorology to assess the
12 growing season accumulation and flux of mercury in a forested ecosystem. Definitions of
13 model constants and constants presented below are summarized in Table 1 and Table 2
14 respectively.

15 2.2 Emission estimates from natural processes in NEI

16 [13] Hg⁰ emission estimates from natural processes in the NEI 2002 inventory used in
17 the BASE case were estimated similar to *Seigneur et al.* [2004] allocating 50% of the
18 annual total (Hg⁰ + Hg²⁺ + PHg) deposition field of a previous simulation to approximate
19 the recycling of deposited mercury and direct emission from mercury enriched
20 landscapes were specified *a priori*. These emission totals were then temporally allocated
21 assuming a diel emission profile based on incoming solar radiation.

22

23 2.3 Review of air-biosphere exchange

1 [14] The scalar flux is typically parameterized in air quality models as the product
2 of the dry deposition velocity and the scalar atmospheric concentration. This assumes that
3 the air-biosphere exchange is in steady state, that biological and chemical sources are
4 absent and that the concentration at the air-surface interface is zero [Businger, 1986];

$$5 \quad F_{\xi} = -V_d \bar{\chi}(z_r) \quad (1)$$

6 where V_d is the deposition velocity and $\bar{\chi}(z_r)$ is the modeled ambient scalar
7 concentration. The deposition velocity is typically estimated using a resistance analogy,
8 note that the sign used here defines positive values as emission and negative values as
9 deposition. The dry deposition velocity parameterization is appropriate for trace gases
10 that are not volatile, but it is unsuitable for modeling the flux of trace gases that readily
11 emit from the air-surface interface due to processes that vary the concentrations inside the
12 surface media [Wesely and Hicks, 2000].

13 [15] The reduction/desorption of mercury species in aqueous and soil matrices has
14 been shown to elevate elemental mercury concentrations in surface waters [Whalin et al.,
15 2007] and in gaseous soil pores [Sigler and Lee, 2006]. Furthermore the documentation
16 of air-vegetation compensation points indicate that reduction/ desorption processes
17 determine the direction of the air-vegetation exchange [Lindberg et al., 2007]. Graydon
18 et al. 2006 documented an air-vegetation compensation point from vegetation that had
19 been spiked with Hg^{2+} stable isotopes at approximately 2 to 3 ng m^{-3} . While Poissant et
20 al. [2008] documented an air-vegetation compensation point at approximately 0.6 ng m^{-3}
21 from an unaltered *Acer saccharum* canopy. Bash and Miller [2009] documented an air-
22 canopy compensation point over an *Acer Rubrum* L. canopy of 1.41 ng m^{-3} using the
23 relaxed eddy accumulation micrometeorological technique. The assumptions used to

1 parameterize Equation (1) are incapable of capturing gradient based compensation point
2 air-surface exchange processes [Wesely and Hicks, 2000].

3 [16] In this study the air-biosphere exchange was parameterized by estimating an
4 atmospheric compensation point as a function of sources and sinks at the air-surface
5 media and using a dynamic compartmentalized model to estimate the scalar canopy (or
6 surface media) storage of $\bar{\chi}$ [Sutton *et al.*, 1998]. The air-surface scalar flux in the
7 vertical direction is estimated following Kaimal and Finnigan [1994] using the flux
8 gradient relationship;

$$9 \quad F_{\xi} = -V_t (\bar{\chi}(z_r) - \bar{\chi}(z_0)) \quad (2)$$

10 where $\bar{\chi}(z_0)$ is the scalar compensation point and V_t is the transfer velocity. V_t is
11 parameterized using a multiple resistance scheme much like V_d as atmospheric and
12 diffusive resistances in bi- and uni-directional exchange are assumed to be the same. The
13 semi-empirical surface resistances to deposition were replaced with semi-empirical
14 partitioning algorithms. In this application, the storage of the scalar in the surface media
15 is parameterized using a dynamic compartmentalized model [Undeman *et al.*, 2009] and
16 $\bar{\chi}(z_r)$ is fully coupled to concentrations in the surface media through the
17 parameterization of $\bar{\chi}(z_0)$. If $\bar{\chi}(z_0)$ is assumed to be negligible in Equation (2), it
18 reduces to the familiar dry deposition velocity parameterization, Equation (1).

19 *2.4 Governing equations of Hg bi-directional model*

20 [17] The general conservation equation of this air-biosphere exchange model is
21 expressed as follows;

$$\frac{d\vec{\chi}(t)}{dt} = \mathbf{K}_{OL}\vec{\chi}(t) + \mathbf{k}_{rxn}\vec{\chi}(t) + \vec{s}(t) \quad (3)$$

where $\vec{\chi}(t)$ is a vector of ambient and near surface mercury Hg^0 and Hg^{2+} concentrations and $\vec{s}(t)$ represents the atmospheric non-gradient dependent sources of Hg^{2+} and Hg^0 , wet deposition, deposited PHg was assumed to be a sink of atmospheric mercury due to a lack of measurements or published mechanisms elucidating the its fate once deposited. \mathbf{K}_{OL} is a matrix of exchange coefficients normalized by flux interface area over the control volume and \mathbf{k}_{rxn} is a matrix of first order linear reactions coefficients currently used to describe the reduction of Hg^{2+} in soil and the surface water Hg redox reactions. Atmospheric mass balance is conserved by passing the net flux of $\vec{\chi}(t)$ in the atmospheric compartment in CMAQ 4.7.

2.4.1 Air-terrestrial exchange

[18] The flux at the air-surface interface over terrestrial systems is parameterized generally following *Sutton et al.* [1998]. Local deposition losses and evasion are used to calculate an atmospheric compensation point. The atmospheric-biosphere flux is driven by a concentration gradient that is defined as the difference between a compensation point and the modeled atmospheric concentration.

$$F_{\text{Hg}^0} = -\frac{1}{\bar{V}_{air}r_a} \left([\text{Hg}^0]_{atm} - [\text{Hg}^0]_{E_0} \right) \quad (4)$$

1 Where F_{Hg^0} is the Hg^0 flux ($\text{mol m}^{-2} \text{s}^{-1}$), \bar{V}_{air} is the molar volume of air at STP, r_a is the
2 atmospheric aerodynamic resistance (s m^{-1}), $[Hg^0]_{z_0}$ is the compensation point at the air-
3 canopy or the air-soil interface (ppm), and $[Hg^0]_{atm}$ is the ambient concentration (ppm).
4 The net canopy compensation point is modeled as a function of air-cuticle, - stomatal and
5 -soil exchange. $[Hg^0]_{z_0}$ is parameterized as a weighted average of the exchange
6 coefficients and fluxes at the atmospheric, cuticular, stomatal, and soil interfaces
7 following *Sutton et al.* [1998].

$$10 \quad [Hg^0]_{z_0} = \frac{\frac{[Hg^0]_{atm}}{r_a} + \frac{[Hg^0]_{st}}{K_{LA}(r_b + r_{st})} + \frac{[Hg^0]_w}{K_{LA}(r_b + r_w)} + \frac{[Hg^0]_{sl,g}}{(r_b + r_{ac} + r_{soil})}}{r_a^{-1} + (r_b + r_{st})^{-1} + (r_b + r_w)^{-1} + (r_b + r_{ac} + r_{soil})^{-1}} \quad (5)$$

11
12 Where $[Hg^0]_{st}$ is the mercury concentration in the apoplastic solution of the leaf (ppm),
13 $[Hg^0]_w$ is the mercury in solution on the cuticular surfaces of the leaf (ppm), $[Hg^0]_{sl,g}$ is
14 the gaseous mercury soil pore space concentration (ppm), r_b is the laminar boundary layer
15 resistance, r_{st} is the stomatal resistance (s m^{-1}), r_m is the mesophyll resistance (s m^{-1}), r_w is
16 the cuticular resistance (s m^{-1}), r_{ac} is the canopy sublayer atmospheric resistance (s m^{-1}),
17 r_{soil} is the soil resistance (s m^{-1}), and K_{LA} is the leaf-air partitioning coefficient for
18 elemental mercury, assumed to be the same for mesophyll and cuticular surfaces. K_{LA} is
19 parameterized using the air-octonal partitioning coefficient for elemental mercury
20 following the framework of *Trapp and Matthies* [1995], described in the following
21 section.

1

2 2.4.2 Air-cuticular exchange

3 [19] The air - cuticular exchange is parameterized following a cuticular
4 capacitance model similar to *Burkhardt et al.* [2009] with partitioning coefficients
5 parameterized following *Trapp and Matthies* [1995];

6

$$7 F_{w,Hg^0} = -\frac{1}{\bar{V}_{air}(r_b + r_w)} \left([Hg^0]_{E_0} - [Hg^0]_w / K_{LA} \right) \quad (6)$$

8

9 where F_{w,Hg^0} is the flux across the air-cuticle interface ($\mu\text{mol m}^{-2} \text{s}^{-1}$).

10

11 2.4.3 Air-stomatal exchange

12

13 [20] Similarly the air - stomatal exchange is parameterized using a big leaf
14 resistance model [*Pleim et al.*, 1996] and the partitioning model of *Trapp and Matthies*
15 [1995];

16

$$17 F_{st,Hg^0} = -\frac{1}{\bar{V}_{air}(r_b + r_{st})} \left([Hg^0]_{E_0} - [Hg^0]_{st} / K_{LA} \right) \quad (7)$$

18

1 where F_{st,Hg^0} is the flux across the air-stomata interface ($\mu\text{mol m}^{-2} \text{s}^{-1}$). Leaf air gas
2 exchange partitioning coefficient, K_{LA} , is parameterized following *Trapp and Matthies*
3 [1995];

$$4 \quad K_{LA} = K_{LW} / H \quad (8)$$

6 where K_{LW} is the leaf water partitioning coefficient, and H is the dimensionless Henry's
7 constant. Mesophyll surfaces are assumed to be coated by a thin film of the apoplast
8 solution and the partitioning is described in Equation (7). The cuticle is assumed to be a
9 sink for mercury except when it is coated with moisture following rain or dew then the
10 cuticular-air partitioning for elemental mercury is assumed to follow Equation (7). The
11 water-vegetation exchange partitioning coefficient, K_{LW} , is estimated following *Trapp*
12 *and Matthies* [1995];

$$14 \quad K_{LW} = (W_p + L_p \rho_o / \rho_l K_{OW}^b) MW_{H_2O} \quad (9)$$

16 where W_p and L_p are the water and lipid content of the plant tissue (fraction mass), K_{OW} is
17 the dimensionless octanol water partitioning coefficient, b is an empirical coefficient used
18 to describe differences in plant lipids, MW_{H_2O} is the molar mass of water and (mol g^{-1})
19 used to convert vegetative concentrations from $\mu\text{mol g}^{-1}$ to $\mu\text{mol mol}^{-1}$, ρ_l and ρ_o are the
20 densities of plant lipids and octanol respectively. b and W_p are species dependent and
21 there are only a handful of measurements available and the value for barley, 0.95 and 0.8
22 respectively, from *Trapp and Matthis* [1995] are applied to the modeling domain. The

1 leaf lipid content reported by *Trapp and Matthies [1995]* , 0.02 g lipids g⁻¹ plant tissue, is
 2 assumed to be representative of the vegetation in the modeling domain. The K_{OW} value
 3 for elemental mercury reported by *Mason et al. [1996]* is used.

4

5 2.4.4 Air-soil exchange

6

7 [21] The air-soil exchange is modeled following *Scholtz et al. [2003]* where the
 8 bulk soil Hg^{2+} concentration is assumed to be constant with respect to the simulation
 9 period, i.e., less than a year.

10

$$11 \quad F_{sl,Hg^0} = -\frac{1}{\bar{V}_{air}(r_{ac} + r_{soil})} \left([Hg^0]_{x_0} - [Hg^0]_{sl,g} \right) \quad (10)$$

12

13 Where F_{sl,Hg^0} is the flux across the air-soil interface ($\mu\text{mol m}^{-2} \text{s}^{-1}$). r_{soil} (s m^{-1}) is
 14 parameterized from the effective diffusion using the Millington-Quirk model as in
 15 *Scholtz et al. [2003]*.

16 The soil air pore concentration is modeled as follows;

17

$$18 \quad [Hg^0]_{sl,g} = \frac{[Hg^0]_{sl,s} MW_{H_2O}}{f_{OC} K_{OC} H MW_{Hg}} \quad (11)$$

19

20 where $[Hg^0]_{sl,s}$ is elemental mercury bound to organic matter in the soil $\mu\text{g g}^{-1}$, f_{OC} is the
 21 fraction of the organic matter in the top 5 cm of the soil, K_{OC} is the dimensionless soil

1 organic matter-water partitioning coefficient, and MW_{Hg} is the molar mass of Hg. The
 2 reduction of soil Hg^{2+} is assumed to follow pseudo first order kinetics at a constant rate of
 3 $k_{r,s} = 8 \times 10^{-11} \text{ s}^{-1}$ following *Scholtz et al.* [2003];

4

$$\begin{aligned}
 \frac{d[Hg^{2+}]_{sl,s}}{dt} &= -k_{r,s} [Hg^{2+}]_{sl,s} \\
 \frac{d[Hg^0]_{sl,s}}{dt} &= k_{r,s} [Hg^0]_{sl,s}
 \end{aligned}
 \tag{12}$$

6 where $[Hg^{2+}]_{sl,s}$ is the Hg^{2+} concentration in the soil matrix. Where $[Hg^{2+}]_{sl,s}$ is assumed
 7 to be constant across the domain at a background concentration of $0.090 \mu\text{g g}^{-1}$ [*Xin et al.*,
 8 2007].

9 2.5 Air-surface water exchange

10

11 [22] The exchange of elemental mercury across the air-water interface is
 12 parameterized using the two-film resistance model of *Slinn et al.* [1978] coupled with the
 13 surface water photo-redox scheme of *Whalin et al.* [2007];

14

$$F_{sw,Hg^0} = -\frac{1}{\bar{V}_{air}(r_a + Hr_l)} \left([Hg^0]_{atm} - [Hg^0]_{aq} H \right)
 \tag{13}$$

16

17 where F_{sw,Hg^0} is the air-surface water Hg^0 flux ($\mu\text{g m}^{-2} \text{ s}^{-1}$), r_l is the liquid side resistance
 18 (s m^{-1}) and $[Hg^0]_{aq}$ is the aqueous phase Hg^0 concentration (ppm). r_l is parameterized as
 19 follows;

$$r_l = \frac{2 Sc^{2/3}}{k (u_*)_w} \quad (14)$$

where k is the von Karman constant (0.4), $(u_*)_w$ is water side friction velocity (m s^{-1})
 $(u_*)_w \approx \rho_a / \rho_w (u_*)_a$, ρ_a and ρ_w are air and water densities (kg m^{-3}) respectively, $(u_*)_a$ is
the atmospheric friction velocity (m s^{-1}), and Sc is the dimensionless Schmidt number for
 Hg^0 .

[23] A surface water photo-redox scheme reported by *Whalin et al.* [2007] is
applied to elemental and divalent mercury species, as noted above. The surface water
compartment was modeled using a layer, assuming a well mixed depth with no horizontal
advection following *Strode et al.* [2007];



where $[\text{Hg}^{2+}]_{aq}$ is the aqueous phase divalent mercury concentration (ppm). The $[\text{Hg}^{2+}]_{aq}$
reduction rate, k_r , of $6.5 \times 10^{-4} \text{ s}^{-1}$ and $[\text{Hg}^0]_{aq}$ oxidation rate, k_o , of $7.2 \times 10^{-4} \text{ s}^{-1}$ of *Whalin*
et al., (2007) were used in the fresh and saltwater photo-redox parameterizations. The
redox rates of *Whalin et al.* [2007] were scaled to modeled incoming solar radiation
following *O'Driscoll et al.* [2006].

18

19 **3. Results and Discussion**

20 [24] Median domain wide Hg^0 concentrations from both cases were similar in
21 magnitude (Figure 1). However, median CMAQ BIDI case concentrations were up to

1 32% lower than the BASE case in western portions of the domain (Figure 2). The largest
2 CMAQ BIDI case Hg^0 increases were around the Gulf of Mexico, increases in median
3 concentrations are as large as 8% (Figures 2 and 3). The bi-directional model did not alter
4 the sources or sinks of Hg^{2+} and PHg species. Thus, changes in their concentrations
5 where driven by the chemical oxidation parameterization and the changes in ambient
6 concentrations of Hg^0 , and generally follow the changes in Hg^0 with a maximum
7 reduction in the median concentration of 7% for Hg^{2+} and 4% for PHg in the western
8 domain and increases of both species of approximately $< 1\%$ for both species around the
9 Gulf of Mexico.

10 [25] In some cases, changes in the pattern of BIDI case diel flux of Hg^0 changed
11 the concentrations of reactive and particulate mercury species even where there was little
12 change in the median ambient atmospheric Hg^0 concentrations due to the modeled
13 oxidation processes in CMAQ. For example, the largest decrease in PHg concentrations
14 was off the coast of Southern California (Figure 3c) where there was little change in the
15 median Hg^0 concentration (Figure 3a). PHg was produced in the CMAQ v4.7 as products
16 of reactions with OH^- and O_3 , where it was assumed that 50% of the products were Hg^{2+}
17 and the remaining 50% were PHg [Pal and Ariya, 2004]. The corresponding decrease in
18 ambient Hg^{2+} concentrations was not as evident because the ocean surface is a stronger
19 sink for Hg^{2+} than fine scale PHg. The recycled emissions in the NEI inventory where
20 assumed to follow a diel cycle and are allocated according to solar irradiance with the
21 highest emission rates at solar noon and with no emissions at night. Atmospheric loading
22 of Hg^0 was in phase with the diel OH^- peak concentration in the BASE case (Figure 4). In
23 the BIDI case, atmospheric evasion of Hg^0 over these coastal areas was driven by the

1 photo reduction of aqueous Hg^{2+} in the surface waters, the ambient Hg^0 concentrations,
2 and the air-sea transfer coefficient, a function of wind speed and temperature. The BIDI
3 case estimated an evasive peak earlier in the morning than the BASE case, which is
4 largely driven by the air-sea transfer coefficient. This shifted the atmospheric loading of
5 Hg^0 out of phase with the diel OH^- peak and thus reduces the PHg concentrations while
6 maintaining similar median Hg^0 concentrations. The reduction of PHg concentrations in
7 this area was largely limited to highest, 95th percentile, PHg concentration episodes
8 (Figure 4).

9 [26] Methylmercury production in watershed has been linked to the net mercury
10 loading (exposure) to the ecosystem [*Harris et al., 2007; Hintelmann et al., 2002*]. Thus
11 the net Hg^0 air-surface exchange to ecosystems from the BASE case was defined as the
12 NEI direct and recycled emission estimates minus the BASE case Hg^0 deposition field.
13 The BIDI case estimated the net air-surface exchange of Hg^0 directly. Note the sign
14 convention used defined the net deposition as negative and net evasion as positive. PHg
15 and Hg^{2+} are not assumed to be evasive and contribute only to the total Hg modeled
16 deposition field. In the BASE case, daily mean Hg^0 air-surface exchange was evasive
17 from a large area in the western United States where NEI emissions from soils that are
18 assumed to be geologically enriched with mercury (Figure 5a and Figure 5b). Mercury
19 evasion from natural processes was generally lower in the western portion of the domain
20 in the BIDI case because legacy mercury contamination and geologically bound mercury
21 were not parameterized. However, BIDI case mercury evasion was larger than the BASE
22 case in around the Gulf Coast and in Eastern Canada (Figure 5). The changes in the mean
23 Hg^{2+} (Figure 6a) and PHg (Figure 6b) dry deposition fields were less sensitive to

1 emissions of Hg^0 from natural process with decreases in mean values up to 8% in the
2 western domain and mean increases up to 3% for both species around the Gulf Coast,
3 generally following the changes in ambient concentrations. Wet deposition of Hg^{2+} and
4 PHg were less sensitive to the changes in the natural emissions estimates than wet
5 deposition estimates of Hg^0 , and generally follows the same pattern as the changes in the
6 ambient concentrations. The total mercury wet deposition decreased by as much as 14%
7 in the western portions of the domain and increased by as much as 1% in South Texas
8 and the in some areas in the Gulf of Mexico (Figure 7).

9 [27] The net air-surface exchange of mercury (i.e., sum of natural emissions - sum
10 of wet and dry deposition), predicted by the BASE case estimated net evasion of mercury
11 from the western portion of the domain during the simulation period while the BIDI case
12 estimated a net deposition to the entire domain with the exception of a small area off the
13 coast of Baja California, where evasion estimated from the initial conditions was greater
14 than the wet and dry deposition inputs (Figure 8). The BIDI case estimated that Hg^0 ratio
15 evasion from terrestrial surfaces and surface waters was 8.5% and 47.8% and the BASE
16 case estimate from surface waters was 52.5% of the total wet and dry deposition over the
17 simulation period, in general agreement with the ratio of deposited stable isotopes
18 estimated to volatilize from terrestrial systems, 8% [Hintelmann *et al.*, 2002] to 30%
19 [Harris *et al.*, 2007], and from aquatic systems, 45% [Harris *et al.*, 2007]. In contrast,
20 the BASE case estimated a much higher rate of cycling from terrestrial systems, 70.4%.
21 Bergquist and Blum [2007] found regional variability in the fraction of mercury volatilized
22 from water bodies indicating that there is a need for more measurements to evaluate the

1 regional variability expressed in ratio of evasion to deposition estimated by air quality
2 models.

3 [28] The BASE and BIDI cases predicted the net hourly exchange rates of Hg^0 of
4 similar magnitudes (Figure 9). However, the evasive flux estimates diverged as the
5 evasive flux rate increases because of the different modeled mechanisms of emission.
6 The bi-directional model predicted evasion when the vegetation and soil pools of mercury
7 elevated the compensation point above the modeled ambient atmospheric concentrations,
8 while NEI direct and recycled estimates are based on a previous model run annual
9 deposition field and *a priori* specified direct background emission temporally allocated to
10 the solar irradiance to approximate the diel emission pattern seen in flux measurements.
11 The NEI method allocated the highest emission rates to areas that experienced the
12 strongest deposition. In areas with consistently high ambient concentrations the NEI
13 estimated high emission rates because the dry deposition field was modeled as the
14 product of the deposition velocity and the ambient concentration, Equation (1), while the
15 gradient approach used the bi-directional model reduced emissions in areas with elevated
16 ambient concentrations, in agreement with recent literature [Fu et al., 2008; Wang et al.,
17 2007; Xin et al., 2007]. The largest deposition events predicted by the model were due to
18 wet deposition of Hg^{2+} species which were relatively insensitive to natural emissions and
19 remain largely unchanged between the models.

20 [29] The BASE case simulation estimated a net flux with evasion of Hg^0
21 exceeding the sum of total wet and dry deposition of Hg species in the Western and
22 Northwestern part of the CONUS domain, Figure 8. Geologically enriched areas are
23 expected to have a higher rate of Hg^0 emissions but published areas of mercury enriched

1 soils do not cover as large an extent as seen in the BASE case and the mobility of the
2 mercury in the soil would be expected to be a function of the soil mineral content [Rytuba
3 2003]. There were several possible reason for this large evasive flux. First, the primary
4 reason for the net evasive Hg^0 flux in the BASE case was the *a priori* specified direct
5 emissions from naturally enriched landscapes. These emissions were too large to balance
6 deposition and oxidative sinks in CMAQ exceeding the total mercury deposition fields by
7 more than 100 fold in some areas and were applied to a large geographic extent (Figure
8 8a). Second, the NEI Hg^0 recycled fields were determined by temporally allocating 50%
9 of a previous model runs total Hg annual deposition field using the incoming radiation to
10 approximate the diel pattern of emissions generally found in the observations. This
11 approximation was not mass consistent due to the feedback of the emissions from non-
12 anthropogenic sources to ambient concentrations and ultimately deposition. Additionally
13 the temporal allocation of the deposition field using incoming solar radiation may not
14 capture the seasonality of net air-surface exchange of mercury. Third, the NEI Hg^0 direct
15 and recycled fields were created from the deposition field from an earlier version of
16 CMAQ with differing chemical mechanisms, boundary conditions and an absence of
17 natural emissions. Changes in model algorithms that impact the deposition fields required
18 the re-compilation of the off-line Hg^0 natural and re-emission fields to approximate the
19 assumption that 50% of the deposited mercury will be re-emitted. Finally, the NEI Hg^0
20 natural and re-emission fields are not constrained by atmospheric and biophysical
21 resistances governing air-surface trace gas exchange. Thus the temporal allocation of
22 natural emission using incoming solar radiation as a proxy may estimate unrealistic
23 evasion rates during time of high irradiation or strong atmospheric stability. The net flux

1 in the western portion of the domain estimates by the BASE case were well above the net
2 flux measurements determined using mass balance techniques reported in the literature
3 [*Graydon et al.*, 2008; *Harris et al.*, 2007; *Hintelmann et al.*, 2002].

4 [30] It is currently estimated that mercury emissions from natural processes range
5 from approximately 40% to 70% of the total mercury loading to the atmosphere [*Shetty et*
6 *al.*, 2008; *Lindberg et al.*, 2007]. The BIDI and BASE case estimates of the net emissions
7 of mercury from natural processes was 71.2% and 84.73% of the total anthropogenic Hg
8 emissions in the modeling domain respectively, Table 3. These estimated ratios are at the
9 high end of the global estimates of Hg⁰ emissions due to natural processes. *Shetty et al.*
10 [2008] estimated that the ratio of Hg⁰ emissions from natural processes to total
11 anthropogenic emissions was greatest during the summer in China when emissions from
12 natural processes were expected to be large. Both the techniques used to estimate
13 emissions from natural processes will estimate less loading in the cool months due to the
14 BASE models parameterization of these emissions as a function of solar radiation and the
15 BIDI models dependence of Henry's constant on temperature, surface water redox
16 parameterization, and ambient concentrations.

17 [31] During the simulation time period, the mercury deposition network wet
18 deposition monitors were the only widely available geographically distributed
19 observations to evaluate regional mercury model simulations in North America.
20 Unfortunately, the modeled wet deposition was not sensitive to the natural emissions
21 given the slow oxidation rates of the relatively insoluble Hg⁰. Wet deposition estimates
22 over the 22 day simulation presented here were similar between the two cases and neither
23 case was significantly better at estimating total wet deposition of mercury. However, the

1 BIDI case had approximately a 2% lower mean bias ($1.08 \mu\text{g m}^{-2}$ or 67.3% versus 1.11
2 $\mu\text{g m}^{-2}$ or 69.4% for the simulation period) than the BASE case, Figure 10. Both cases
3 were subject to overprediction of precipitation, mean normalized bias of 18.6% and $r^2 =$
4 0.373 , between MM5 estimated and observed precipitation at MDN sampling sites during
5 the simulation period. An annual simulation is in preparation to assess the seasonal
6 dynamics of the BASE and BIDI model cases against MDN observations.

7 [32] A five month box model simulation of was run using Hg and Hg^{2+}
8 concentrations and meteorology from the BASE model, mean of 1.21 ng m^{-3} and 43.5 pg
9 m^{-3} respectively, repeated for five months to simulate the variability of the ambient
10 concentrations and meteorology from a central Connecticut grid cell. The land cover type
11 was specified as a hardwood forest with a leaf area index of 5.3 with an assumed leaf dry
12 mass of 370 g. The air-canopy compensation point ranged from 0.99 ng m^{-3} for the first
13 month and leveled off at 1.29 ng m^{-3} during the third month of the simulation, all within
14 recently published ranges [Bash and Miller, 2009; Poissant et al., 2008; Graydon et al.,
15 2006]. Mercury fluxes ranged from -5.8 to $1.9 \text{ ng m}^{-2} \text{ h}^{-1}$ with the largest deposition rates
16 during the first month of the simulation. Mercury accumulated in the modeled vegetation
17 at a rate of $0.26 \text{ ng g}^{-1} \text{ day}^{-1}$, 39.93 ng g^{-1} total accumulation over the simulation, in
18 agreement with the measurements of Bushey et al. [2008], ranging form 0.22 to 0.35 ng
19 $\text{g}^{-1} \text{ day}^{-1}$ with a total accumulation of $37.3 \pm 12.4 \text{ ng g}^{-1}$. Hg^0 accumulation leveled off at
20 approximately 2.65 ng g^{-1} after the third month of the simulation and the remainder of the
21 estimated mercury accumulation was due to Hg^{2+} deposition. This simulation was used to
22 examine the models seasonality over a growing season and conduct a sensitivity of the
23 air-vegetation partitioning scheme. W_p , l_m , l_c , and b from Equation 9 were varied by

1 ±20% and with all sensitivities resulting in less than a 1% change in the flux with the
2 magnitude of the flux being most sensitive to the resistance terms rather than the
3 partitioning terms. The magnitude of the flux was not sensitive to changes of ±20% in
4 K_{LW} but the total accumulation of Hg^0 in the canopy was more sensitive to this variable a
5 20% increases resulted in approximately 19.4% increase in accumulation of Hg^0 (1.3%
6 increase in the total mercury accumulation and net growing season deposition to the
7 canopy).

8 **4. Conclusion**

9 [33] A dynamic compartmentalized air-surface exchange model for mercury has
10 been developed for CMAQ based on a resistance surface exchange model coupled to a
11 compartmentalized multimedia model. This model has expanded the processes
12 mechanistically parameterized by CMAQ and improved model estimates of the net air-
13 biosphere exchange of mercury. The air-surface fluxes were constrained by the
14 atmospheric and biophysical resistances governing near surface trace gas exchange and
15 the mass balance of mercury species in the surface media.

16 [34] BIDI and BASE case simulations were run for one month to assess the bi-
17 directional parameterization against an evaluated model. Domain-wide, these changes
18 reduced ambient median Hg^0 concentrations by only 2.2%, but ranged from 185% to 33%
19 of the BASE case concentrations, i.e., increased spatial heterogeneity. The THg
20 deposition fields to the eastern half of the domain were similar. However, the magnitude
21 and temporal variability of the Hg^0 deposition field was more dynamic in the bi-
22 directional model. The air-surface media coupling in the in-line air-surface exchange
23 model was based on mechanistic processes and can dynamically adapt to changes in

1 ambient concentration during the model run or changes to model configurations, i.e.,
2 updated chemical mechanisms, emission inventories, and boundary conditions. Previous
3 methods of estimating emissions from natural processes required a recompilation of the
4 natural emissions for each case to approximate the assumption that a fraction of the total
5 mercury deposited that is re-emitted [*Silen et al.*, 2008; *Seigneur et al.*, 2004], that
6 mercury is transported from the soil water pool to the atmosphere *via* transpiration and
7 empirically-based soil emission models without any atmospheric feedback [*Gbor et al.*,
8 2006; *Lin et al.*, 2005; *Bash et al.*, 2004; *Xu et al.*, 1999], or that a fraction of the mercury
9 deposited is instantaneously re-emitted [*Silen et al.*, 2008].

10 [35] The bi-directional Hg exchange module in CMAQ estimated mercury
11 emissions from natural processes that were more consistent with observations, the current
12 understanding of the net air-biosphere exchange of mercury and backed by more robust
13 theory governing the air-surface exchange of semi-volatile pollutants. Even with
14 empirical estimates of partitioning coefficients and redox mechanisms and assumed
15 domain wide vegetation and soil parameters, a one month run of CMAQ with and
16 without bi-directional mercury exchange clearly show that the bi-directional model
17 detailed here improved the net mercury exchange estimates over a widely used emissions
18 inventory. It should be noted that there is considerable uncertainty in the air-vegetation
19 partitioning and soil reduction schemes adapted here and experiments have not yet been
20 devised to estimate the relative contribution of Hg^0 and Hg^{2+} to vegetation. Future
21 measurements of the air-vegetation and -soil exchange, concentrations of mercury in
22 environmental media, and the determination of surface reduction and oxidation processes
23 will facilitate more complete model evaluation and will better constrain a

1 compartmentalized multimedia model of air-biosphere exchange which will further
2 constrain modeled flux estimates and result in future model improvements.

3

4 [36] **Disclaimer:** *The United States Environmental Protection Agency through its Office of*
5 *Research and Development funded and managed the research described here. It has been*
6 *subjected to Agency's administrative review and approved for publication.*

1 **5. Literature Cited**

2

3 Bash, J.P. and D.R. Miller (2009), Growing season total gaseous mercury (TGM) flux
4 measurements over an *Acer rubrum* L. stand. *Atmos. Environ.* 43, 5953-5961

5

6 Bash, J.O., P. Bresnahan, D.R. Miller (2007), Dynamic surface interface exchanges of
7 mercury: a review and compartmentalized modeling framework. *J. Appl. Meteorol.*
8 *Clim.* 46, 1606-1618

9

10 Bash, J.O., D.R., Miller, T.H. Meyer, P.A. Bresnahan (2004), Northeast United States
11 and Southeast Canada natural mercury emissions estimated with a surface emission
12 model. *Atmos. Environ.*, 38, 5683-5692

13

14 Bergquist, B.A., J.D. Blum (2007), Mass-dependent and -independent fractionation of Hg
15 isotopes by photoreduction in aquatic systems. *Science* 318, 417-420

16

17 Bullock, O.R., D. Atkinson, T. Braverman, K. Civerolo, A. Dastoor, D. Davingnon, J.Y.

18 Ku, K. Lohman, T.C. Myers, R.J. Park, C. Seigneur, N.E. Selin, G. Sistla, K.

19 Vijayaraghavan (2009), An analysis of simulated wet deposition of mercury from the

20 North American Mercury Model Intercomparison Study. *J. Geophys. Res.* 114,

21 D08301

22

1 Bullock, O.R., D. Atkinson, T. Braverman, K. Civerolo, A. Dastoor, D. Davignon, J.Y.
2 Ku, K. Lohman, T.C. Myers, R.J. Park, C. Seigneur, N.E. Selin, G. Sistla, K.
3 Vijayaraghavan (2008), The North American Mercury Model Intercomparison Study
4 (NAMMIS): study description and model-to-model comparisons. *J. Geophys. Res.*
5 113, D17310
6
7 Bullock, O.R., K.A. Brehme (2002), Atmospheric mercury simulation using the CMAQ
8 model: formulation description and analysis of wet deposition results. *Atmos.*
9 *Environ.* 36, 2135-2146
10
11 Burkhardt, J., C.R. Flechard, F. Gressens, M. Mattsson, P.A.C. Jonejan, J.W. Erisman, T.
12 Weidinger, R. Meszaros, E. Nemitz, M.A. Sutton (2009), Modelling the dynamic
13 chemical interactions of atmospheric ammonia with leaf surface wetness in a
14 managed grassland canopy. *Biogeosci.* 6, 67-84
15
16 Bushey, J.T., A.G. Nallana, M.R. Montesdeoca, C.T. Driscoll (2008), Mercury dynamics
17 of a northern hardwood canopy. *Atmos. Environ.* 42, 6905-6914
18
19 Businger, J.A. (1986), Evaluation of the accuracy with which dry deposition can be
20 measured with current micrometeorological techniques. *J. Clim. Appl. Meteorol.* 25,
21 1100-1124
22

1 Byun, D., K.L. Schere (2006), Review of the governing equations, computational
2 algorithms, and other components of the Models-3 Community Multiscale Air
3 Quality (CMAQ) modeling system. *Appl. Mech. Rev.* 59, 51-77
4
5 Carlton, A.G., B.J. Turpin, K.E. Altieri, S.P. Seitzinger, R. Mathur, S.J. Roselle, R.J.
6 Weber (2008), CMAQ model performance enhanced when in-cloud secondary
7 organic aerosol is included: comparisons of organic carbon predictions with
8 measurements. *Environ. Sci. Technol.* 42, 8798-8802
9
10 Carlton, A.G., P.V. Bhave, S. Napelenok, G. Pouliot, R.W. Pinder, G. Sarwar, M.
11 Houyoux, (*submitted*), Improved treatment of secondary organic aerosol in CMAQ.
12 *Environ. Sci. Technol.*
13
14 Fitzgerald, W.F., D.R. Engstrom, R.P. Mason, E.A. Nater (1998), The case for
15 atmospheric mercury contamination in remote areas. *Environ. Sci. Technol.* 32, 1-7
16
17 Flechard, C.R., D. Fowler, J.N. Cape (1999), A dynamic chemical model of bi-directional
18 ammonia exchange between semi-natural vegetation and the atmosphere. *Q. J. R.*
19 *Meteorol. Soc.* 125, 2611-2641
20
21 Fu, X., X. Feng, S. Wang (2008), Exchange fluxes of Hg between surfaces and
22 atmosphere in the eastern flank of Mount Gongga, Sichuan province,
23 southwestern China. *J. Geophys. Res.* 113, D20306

1

2 Gbor, P.K., D. Wen, F. Meng, F. Yang, B. Zhang, J.J. Sloan (2006), Improved model for
3 mercury emission, transport and deposition, *Atmos. Environ.*, 40, 973-983
4

5 Graydon, J.A., V.L. St. Louis, H. Hintelmann, S.E. Lindberg, K.A. Sandilands, J.W.M.
6 Rudd, C.A. Kelly, B.D. Hall, L.D. Mowat (2008), Long-term wet and dry deposition
7 of total and methyl mercury in the remote boreal ecoregion of Canada, *Environ. Sci.*
8 *Technol.*, 42, 8345-8351
9

10 Graydon, J.A., V.L. St. Louis, S.E. Lindberg, H. Hintelmann, D.P. Krabbenhoft (2006),
11 Investigation of mercury exchange between forest canopy vegetation and the
12 atmosphere using a new dynamic chamber. *Environ. Sci. Technol.* 40, 4680-4688
13

14 Grell, G., J. Dudhia, D. Stauffer (1994), A description of the fifth-generation Penn
15 State/NCAR mesoscale model (MM5), NCAR Tech. Note NCAR/TN-398+STR,
16 National Center for Atmospheric Research, Boulder, CO.
17

18 Harris, R.C., J.W.M. Rudd, M. Amyot, C.L. Bariariz, K.G. Beaty, P.J. Blanchfield, R.A.
19 Bodaly, B.A. Branfireun, C.C. Gilmour, J.A. Graydon, A. Heyes, H. Hintelmann,
20 J.P. Hurley, C.A. Kelly, D.P. Krabbenhoft, S.E. Lindberg, R.P. Mason, M.J.
21 Paterson, C.L. Podemski, A. Robinson, K.A. Sandilands, G.R. Southworth, V.L. St.
22 Louis, M.T. Tate (2007) Whole-ecosystem study shows rapid fish-mercury response
23 to changes in mercury deposition. *Proc. Natl. Acad. Sci. USA* 104, 16586-16591

1
2 Hammerschmidt, C.R., W.F. Fitzgerald (2006), Methylmercury in freshwater fish linked
3 to atmospheric mercury deposition, *Environ. Sci. Technol.* 40, 7764-7770
4
5 Hedgecock, I.M., N. Pirrone (2004), Chasing quicksilver: modeling the atmospheric
6 lifetime of $\text{Hg}^0_{(g)}$ in the marine boundary layer at various latitudes. *Environ. Sci.*
7 *Technol.* 38. 69-76
8
9 Hertel, O., R. Berkowicz, J. Christensen, Ø. Hov (1993), Test of two numerical schemes
10 for use in atmospheric transport-chemistry models. *Atmos. Environ.* 27A, 2591-2611
11
12 Hintelmann, H., R. Harris, A. Heyes, Hurley, C.A. Kelly, D.P. Krabbenhoft, S. Lindberg,
13 J.W.M. Rudd, K.J. Scott, V.L. St.Louis (2002), Reactivity and mobility of new and
14 old mercury deposition in a boreal forest ecosystem during the first year of the
15 METAALICUS study, *Environ. Sci. Tehnol.* 36, 5034-5040
16
17 Houyoux, M.R., J.M. Vukovich, C.J Coats Jr., N.J.M. Wheeler, P.S. Kasibhatla (2000),
18 Emission inventory development and processing for the seasonal model for regional
19 air quality (SMRAQ) project, *J. Geophys. Res.* 105(D7), 9079-9090
20
21 Kaimal, J.C. and J.J. Finnigan (1994), *Atmospheric boundary layer flows: their structure*
22 *and measurement*, Oxford University Press, New York, NY, 289 pp
23

1 Lin, C-J., S.E. Lindberg, T.C. Ho, C. Jang (2005), Development of a processor in BEIS3
2 for estimating vegetative mercury emissions in the continental United States. *Atmos.*
3 *Environ.* 39: 7529-7540
4
5 Lindberg, S.E., R. Bullock, R. Ebinghaus, D. Engstrom, X. Feng, W. Fitzgerald, N.
6 Pirrone, E. Prestbo, C. Seigneur (2007), A synthesis of progress and uncertainties in
7 attributing the sources of mercury in deposition, *Ambio* 36: 19-32
8
9 Lindberg, S.E. and S. Vermette (1995), Workshop on sampling mercury in precipitation
10 for the national atmospheric deposition program. *Atmos. Environ.* 29, 1219-1220
11
12 Mason, R.P., J.R. Reinfelder, F.M.M. Morel (1996), Uptake, toxicity, and trophic transfer
13 of mercury in a coastal diatom, *Environ. Sci. Technol.* 30, 1835-1845
14
15 O'Driscoll, N.J., S.D. Siciliano, D.R.S. Lean, M. Amyot (2006), Gross photoreduction
16 kinetics of mercury in temperate freshwater lakes and rivers: application of a general
17 model of DGM dynamics, *Environ. Sci. Technol.* 40, 837-843
18
19 Orihel, D.M., M.J. Paterson, P.J. Blanchfield, R.A. Bodaly, H. Hintelmann (2007),
20 Experimental evidence of a linear relationship between inorganic mercury loading
21 and methylmercury accumulation by aquatic biota, *Environ. Sci. Technol.* 41, 4952-
22 4958
23

1 Pal, B. and Ariya, P.A., (2004), Gas-phase HO[•]-initiated reactions of elemental mercury:
2 Kinetics, product studies, and atmospheric implications. *Environ. Sci. Technol.* 38,
3 5555-5566
4

5 Pleim, J.E. and A. Xiu (1995), Development and testing of a surface flux and planetary
6 boundary-layer model for application in mesoscale models. *J. Appl. Meteorol.* 34,
7 16-32
8

9 Pleim, J.E., J.F. Clarke, P.L. Finkelstein, E.J. Cooter, T.G. Ellestad, A. Xiu, W.M.
10 Angevine (1996), Comparison of measured and modeled surfaces fluxes of heat,
11 moisture and chemical dry deposition. In: *Air pollution modeling and its application*
12 *XI*, eds: Gryning, Schiermeier, Plenum, New York
13

14 Poissant, L., M. Pilote, E. Yumvihoze, D. Lean (2008), Mercury concentrations and
15 foliage/atmosphere fluxes in a maple forest ecosystem in Quebec, Canada. *J.*
16 *Geophys. Res.* 113, D10307
17

18 Ryaboshapko, A., O.R. Bullock, J. Christensen, M. Cohen, A. Dastoor, I. Ilyin, G.
19 Petersen, D. Syrakov, O. Travnikov, R.S. Artz, D. Davignon, R.R. Draxler, J.
20 Munthe, J. Pacyna (2007a), Intercomparison study of atmospheric mercury models:
21 2. Modeling results vs. long-term observations and comparison of country deposition
22 budgets. *Sci Tot. Environ.* 377, 319-333
23

1 Ryaboshapko, A., O.R. Bullock, J. Christensen, M. Cohen, A. Dastoor, I. Ilyin, G.
2 Petersen, D. Syrakov, O. Travnikov, R.S. Artz, D. Davignon, R.R. Draxler, J.
3 Munthe (2007b), Intercomparison study of atmospheric mercury models: 1.
4 Comparison of models with short-term measurements. *Sci. Tot. Environ.* 376, 228-
5 240
6
7 Rytuba, J.J (2003), Mercury from mineral deposits and potential environmental impact.
8 *Environ. Geol.* 43, 326-338
9
10 Sarwar, G., D. Luecken, G. Yarwood, G.Z. Whitten, W.P.L. Carter (2008), Impact of an
11 updated carbon bond mechanism on predictions from the CMAQ modeling system:
12 preliminary assessment, *J. Appl. Meteorol. Clim.* 47, 3-14
13
14 Selin, N.E., D.J. Jacob, R.M. Yantosca, S. Strode, L. Jaeglé, E.M. Sunderland (2008),
15 Global 3-D land-ocean-atmosphere model for mercury: present day versus
16 preindustrial cycles and anthropogenic enrichment factors for deposition. *Glob.*
17 *Biogeochem. Cycles*, 22, doi:10.1029/2007GB003040
18
19 Scholtz, M.T., B.J. Van Heyst, W.H. Schroeder (2003), Modelling of mercury emissions
20 from background soils, *Sci. Tot. Environ.* 304, 185-207
21

1 Seigneur, C., P. Karamchandani, K. Lohman, K. Vijayaraghavan (2001), Multiscale
2 modeling of atmospheric fate and transport of mercury. *J. Geophys. Res.* 106(D21),
3 27795-27809
4
5 Seigneur, C., K. Vijayaraghavan, K. Lohman, P. Karamchandani, C. Scott (2004), Global
6 source attribution for mercury deposition in the United States, *Environ. Sci. Technol.*
7 38, 555-569
8
9 Shetty, S.K., C.J. Lin, D.G. Streets, C. Jang (2008), Model estimates of mercury
10 emissions from natural sources in East Asia, *Atmos. Environ.* 37, 8674-8685
11
12 Sigler, J.M. and X. Lee (2006), Gaseous mercury in background forest soil in the
13 northeastern United States, *J. Geophys. Res.* 111, G02007
14
15 Seinfeld, J.H. and S.N. Pandis (1998), *Atmospheric Chemistry and Physics: From Air*
16 *Pollution to Climate Change*. John Wiley, New York.
17
18 Slinn, W.G.N, L. Hasse, B.B. Hicks, A.W. Hogan, D. Lal, P.S. Liss, K.O. Munnich, G.A.
19 Sehmel, O. Vittori (1978), Some Aspects of the transfer of atmospheric trace
20 constituents past the air-sea interface. *Atmos. Environ.* 12, 2055-2087
21

1 Strode, S.A., L. Jaegle, N.E. Selin, D.J. Jacob, R.J. Park, R.M. Yantosca, R.P. Mason, F.
2 Slemr (2007), Air-sea exchange in the global mercury cycle, *Global Biogeochem.*
3 *Cycles* 21, GB1017
4
5 Sunderland, E.M. (2007), Mercury exposure from domestic and imported estuarine and
6 marine fish in the U.S. seafood market. *Environ. Health. Perspect.* 112, 562-570
7
8 Sutton, M.A., J.K. Burkhardt, D. Guerin, E. Nemitz, D. Fowler (1998), Development of
9 resistance models to describe measurements of bi-directional ammonia surface-
10 atmosphere exchange. *Atmos. Environ.* 32, 473-480
11
12 Trapp, S. (2004), Plant uptake and transport models for neutral and ionic chemicals,
13 *Environ. Sci. Pollut. Res.* 11(1), 33-39
14
15 Trapp, S. and M. Matthies (1995), Generic one-compartment model for uptake of organic
16 chemicals by foliar vegetation. *Environ. Sci. Technol.* 29, 2333-2338
17
18 Undeman, E., G. Czub, M.S McLachlan (2009), Addressing temporal variability when
19 modeling bioaccumulation in plants. *Environ. Sci. Technol.* 43, 3751-3756
20
21 U.S. EPA (1997), Mercury study report to congress, EPA-452-R-97-004
22

1 Vermette S., S.E. Lindberg, N. Bloom (1995), Field tests for a regional mercury
2 deposition network – sampling design and preliminary test results. *Atmos. Environ.*
3 29, 1247-1251
4

5 Wang, S., X. Feng, G. Qui, X. Fu, Z. Wei (2007), Characteristics of mercury exchange
6 flux between soil and air in heavily air-polluted are, eastern Guizhou, China, *Atmos.*
7 *Environ.* 41(27), 5584-5594
8

9 Wesely, M.L. and B.B. Hicks (2000), A review of the current status of knowledge in dry
10 deposition in regional-scale numerical models. *Atmos. Environ.* 34, 4345-4355
11

12 Weiss-Penzias, P., D.A. Jaffe, A. McClintick, E.M. Prestbo, M.S. Landis (2003),
13 Gaseous elemental mercury in the marine boundary layer: evidence for rapid
14 removal in anthropogenic pollution. *Environ. Sci. Technol.*, 37, 3755-3763
15

16 Whalin, L, E.-H. Kim, R. Mason (2007), Factors influencing the oxidation, reduction,
17 methylation and demethylation of mercury species in coastal water, *Marine Chem.*
18 107:278-294
19

20 Wolfe, M.F., S. Schwarzbach, R.A. Sulaiman (1998) Effects of mercury on wildlife: a
21 comprehensive review. *Environ. Toxicol. Chem.* 17, 146-160
22

- 1 Xin, M., M. Gustin, D. Johnson (2007), Laboratory investigation of the potential for re-
2 emission of atmospherically derived Hg from soils. *Environ. Sci. Technol.* 41, 4946-
3 4951
4
- 5 Xu, X., X. Yang, D.R. Miller, J.J. Helble, R.J. Carley (1999), Formulation of bi-
6 directional atmosphere-surface exchanges of elemental mercury. *Atmos. Environ.* 34,
7 4933-4944

1 List of Tables

2

3 **Table 1. Constants and rates used in the bi-directional mercury exchange model.**

4

5 **Table 2. Model variables and units in the bi-directional mercury exchange model.**

6

7 **Table 3. CONUS domain wide estimates of mercury deposition, emissions (Emis.) and net air-surface**
8 **exchange (ASX).**

9

10 List of Figures

11

12 **Figure 1, resistance diagram of CMAQ with unidirectional exchange (a) and bi-directional exchange**
13 **(b), $R_{i,j}$ are resistances, arrows indicated the direction of mass transport, $C_{i,s}$ are surface**
14 **capacitances, and the remaining variables are defined in Table 2.**

15

16 **Figure 2, BASE (a) and BIDI (b) median ambient layer one elemental mercury concentration**
17 **estimates.**

18

19 **Figure 3, median of the ratio of the BIDI to BASE case mercury concentrations for BIDI/BASE Hg^0**
20 **(a), BIDI/BASE Hg^{2+} (b) and BIDI/BASE PHg (c) from July 10th to July 31st 2002. The black contour**
21 **lines denotes the area where the BIDI = BASE case concentrations.**

22

23 **Figure 4, BIDI (a) and BASE (b) case Hg^0 air-sea flux, BIDI (grey) and BASE (black) PHg ambient**
24 **concentrations (c) and OH ambient concentrations (d). The symbols are defined as: \oplus 5th, ∇ 25th, \circ**
25 **median, Δ 75th, and \oplus 95th percentiles.**

26

1 **Figure 5, mean daily net air surface exchange of elemental mercury from July 10th through the 31st**
2 **for the BASE case (a) and BIDI case (b), positive values indicate net evasion and negative values**
3 **indicate net deposition, separated by the white contour line**

4
5 **Figure 6, The mean ratio of the BIDI case to the BASE case total dry deposition of Hg²⁺ (a) and PHg**
6 **(b), The black contour lines denotes the area where the BIDI = BASE case mean dry deposition.**

7
8 **Figure 7, Ratio of BIDI to BASE case wet deposition estimates of Hg⁰ (a), Hg²⁺ (b), PHg (c), and total**
9 **Hg (d) from July 10th through the 31st, black contour lines denotes the area where the BIDI = BASE**
10 **case mean dry deposition.**

11
12 **Figure 8, Ratio of total Hg⁰ evasion from natural processes to total mercury wet and dry deposition**
13 **estimated by the BASE case (a) and the BIDI case (b) from July 10th through the 31st. Black contour**
14 **lines encompass areas where Hg⁰ evasion exceeds the total mercury loading.**

15
16 **Figure 9, Total mercury surface exchange estimates from CMAQ 4.7 plotted against CMAQ 4.7 with**
17 **bi-directional mercury exchange for hourly flux estimates (a) and the mean daily flux over the**
18 **simulation period (b).**

19
20 **Figure 10, Simulated total mercury wet deposition (a) and total precipitation (b) and plotted against**
21 **observed values at Mercury Deposition Network monitors for BASE (circles) and BIDI (triangles)**
22 **cases.**

1 **Table 1. Constants and rates used in the bi-directional mercury exchange model.**

Constants		Values	Reference
\bar{V}_{air}	Molar volume of air at STP	$22.414 \times 10^{-3} \text{ m}^3 \text{ mol}^{-1}$	<i>Seinfeld and Pandis 1998</i>
W_p	Ratio of leaf water content to leaf mass	0.80 (g/g)	<i>Trapp and Matthies 1995</i>
L_p	Ratio of leaf lipid content to leaf mass	0.02 (g/g)	<i>Trapp and Matthies 1995</i>
ρ_o	Density of octanol	0.822 (kg/l)	<i>Trapp and Matthies 1995</i>
ρ_l	Density of water	1.000 (kg/l)	<i>Trapp and Matthies 1995</i>
K_{OW}	Hg ⁰ octanol-water partitioning coefficient	4.15 (Dimensionless)	<i>Mason et al. 1996</i>
b	Empirical	0.95 (Dimensionless)	<i>Trapp and Matthies 1995</i>
K_{OC}	Hg ⁰ /Hg ²⁺ water-organic matter partitioning coefficient	20/100 (Dimensionless)	<i>Schultz et al. 2003</i>
$k_{r,s}$	Reduction rate of divalent soil mercury	$8 \times 10^{-11} \text{ (s}^{-1}\text{)}$	<i>Schultz et al. 2003</i>
k_r	Photo-reduction rate of divalent mercury in surface waters	$6.5 \times 10^{-4} \text{ (s}^{-1}\text{)}$	<i>Whalin et al. 2007</i>
k_o	Photo-oxidation rate of divalent mercury in surface waters	$7.2 \times 10^{-4} \text{ (s}^{-1}\text{)}$	<i>Whalin et al. 2007</i>
$[Hg^{2+}]_{sl,s}$	Bulk Soil Hg ²⁺ concentrations	0.090 ($\mu\text{g g}^{-1}$)	<i>Xin et al. 2007</i>

2

1 **Table 2. Model variables and units in the bi-directional mercury exchange model.**

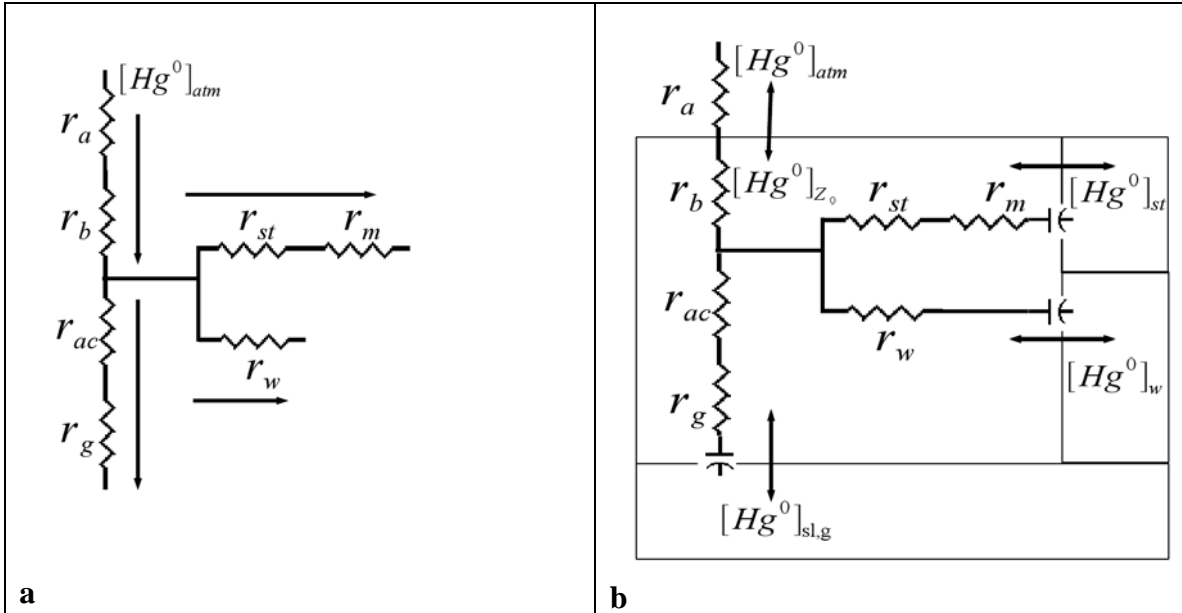
Model Variables		Units
$\bar{\chi}(z_r)$	Atmospheric scalar concentration at z_r	ppm
$\bar{\chi}(z_0)$	Scalar compensation point	ppm
F_{Hg^0}	Air-surface exchange of Hg^0	$\mu\text{mol m}^{-2} \text{s}^{-1}$
F_{w,Hg^0}	Air-cuticular exchange of Hg^0	$\mu\text{mol m}^{-2} \text{s}^{-1}$
F_{st,Hg^0}	Air-stomatal exchange of Hg^0	$\mu\text{mol m}^{-2} \text{s}^{-1}$
F_{soil,Hg^0}	Air-soil exchange of Hg^0	$\mu\text{mol m}^{-2} \text{s}^{-1}$
$[Hg^0]_{z_0}$	Canopy Hg^0 compensation point	ppm
$[Hg^0]_{atm}$	Ambient Hg^0 concentration	ppm
$[Hg^0]_{st}$	Hg^0 in leaf mesophyll reservoir	$\mu\text{mol g}^{-1}$ leaf dry mass
$[Hg^0]_w$	Hg^0 bound to leaf cuticular surfaces	$\mu\text{mol g}^{-1}$ leaf dry mass
$[Hg^0]_{sl,g}$	Gaseous Hg^0 concentration in soil pore spaces	ppm
$[Hg^0]_{aq}$	Surface water Hg^0 concentration	$\mu\text{mol mol}^{-1}$
$[Hg^0]_{sl,s}$	Sorbed Soil Hg^0 concentrations	$\mu\text{g g}^{-1}$
$[Hg^{2+}]_{aq}$	Surface water Hg^{2+} concentration	$\mu\text{mol mol}^{-1}$
r_a	Aerodynamic resistance	s m^{-1}
r_b	Boundary layer resistance	s m^{-1}
r_{st}	Stomatal resistance	s m^{-1}
r_w	Cuticular resistance	s m^{-1}
r_{ac}	In-canopy aerodynamic resistance	s m^{-1}
r_{soil}	Resistance to soil diffusion	s m^{-1}
r_l	Liquid side air-water resistance	s m^{-1}
V_d	Deposition velocity	m s^{-1}
V_t	Transfer velocity	m s^{-1}
K_{LA}	Leaf air portioning coefficient	mol air g^{-1} leaf dry mass
K_{LW}	Leaf air water portioning coefficient	mol water g^{-1} leaf dry mass
f_{OC}	Fraction of soil organic matter	%
H	Henry's constant	Dimensionless
Modeled Matrices and vectors		Description
\mathbf{K}_{OL}		Matrix of exchange coefficients
\mathbf{k}_{rxn}		Matrix of reaction coefficients
$\vec{\chi}(t)$		Vector of scalar concentrations
$\vec{s}(t)$		Vector of sources and sinks

1 **Table 3. CONUS domain wide estimates of mercury deposition, emissions (Emis.) and net air-surface**
 2 **exchange (ASX).**

	BASE			BIDI		
	Mg month ⁻¹	% ASX	% Emis.	Mg month ⁻¹	% ASX	% Emis.
Hg ⁰ Wet Deposition	-0.01	0.02%	-	-0.01	0.01%	-
Hg ²⁺ Wet Deposition	-42.64	82.62%	-	-42.02	62.86%	-
PHg Wet Deposition	-2.44	4.73%	-	-2.39	3.58%	-
Hg ⁰ Dry Deposition ¹	-14.58	28.25%	-	-	-	-
Hg ⁰ Evasion from natural sources ²	41.77	-80.93%	130.17%	-	-	-
Net Hg ⁰ Air-Surface Exchange	27.19	-52.68%	84.73%	10.68	-15.98%	71.20%
Hg ²⁺ Dry Deposition	-33.57	65.05%	-	-32.97	49.32%	-
PHg Dry Deposition	-0.14	0.27%	-	-0.14	0.21%	-
Total Air-Surface Exchange	-51.61	100.00%	-	-66.85	100.00%	-
NEI Hg ⁰ Anthropogenic Emissions	3.16	-	9.85%	3.16	-	21.07%
NEI Hg ²⁺ Anthropogenic Emissions	0.75	-	2.34%	0.75	-	5.00%
NEI PHg Anthropogenic Emissions	0.41	-	1.28%	0.41	-	2.73%
Total Emissions ³	32.09	-	100.00%	15.00	-	100.00%

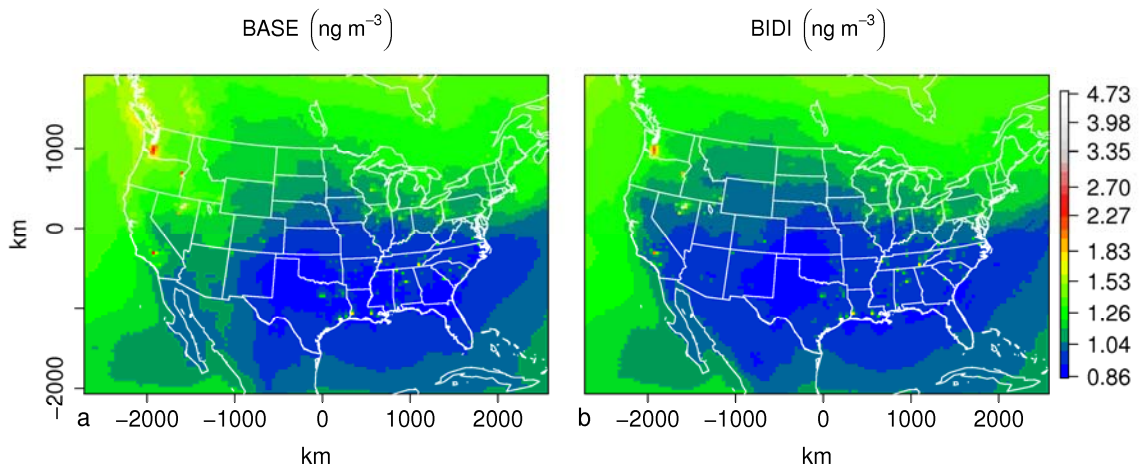
3 1. CMAQ modeled Hg⁰ dry deposition component of the net air-surface exchange, 2. NEI modeled evasion
 4 from natural sources. 3. Total emissions are defined as the sum net Hg⁰ air-surface exchange and
 5 anthropogenic Hg emissions

1



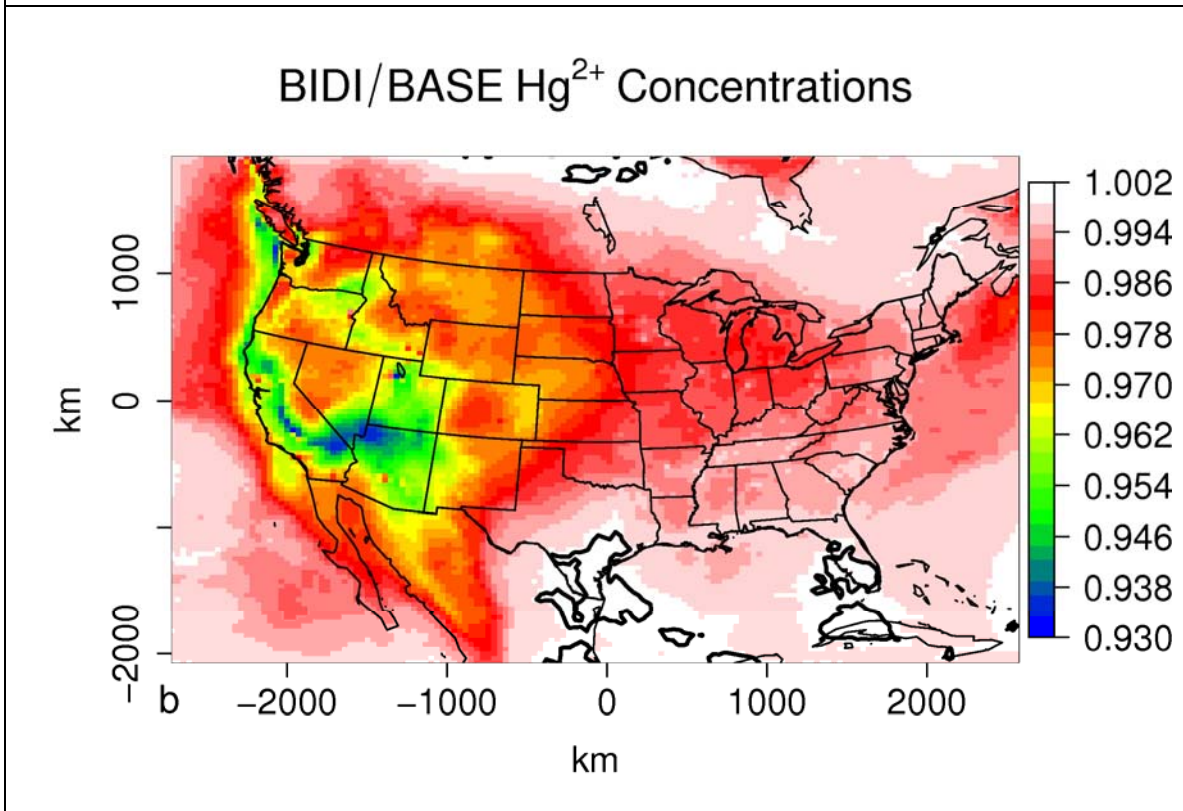
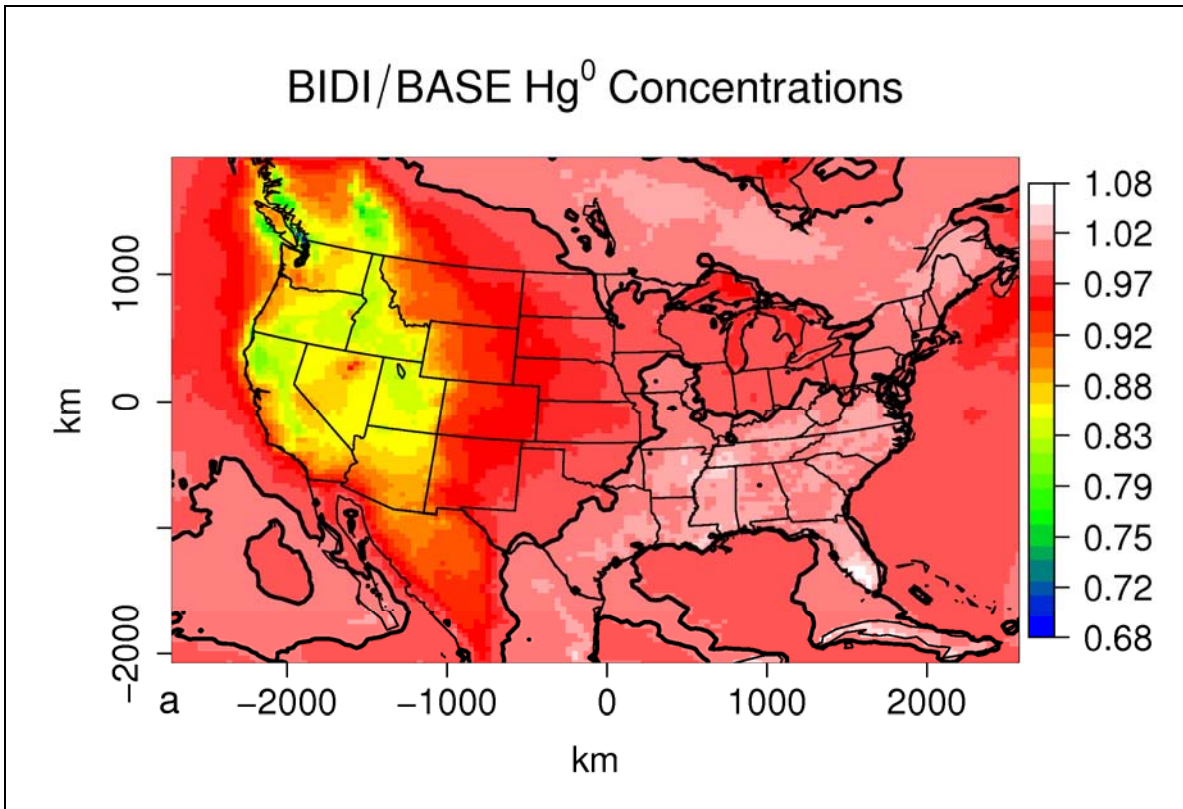
2 **Figure 4, resistance diagram of CMAQ with unidirectional exchange (a) and bi-directional exchange**
 3 **(b), \sim are resistances, arrows indicated the direction of mass transport, \lrcorner are surface**
 4 **capacitances, and the remaining variables are defined in Table 2.**

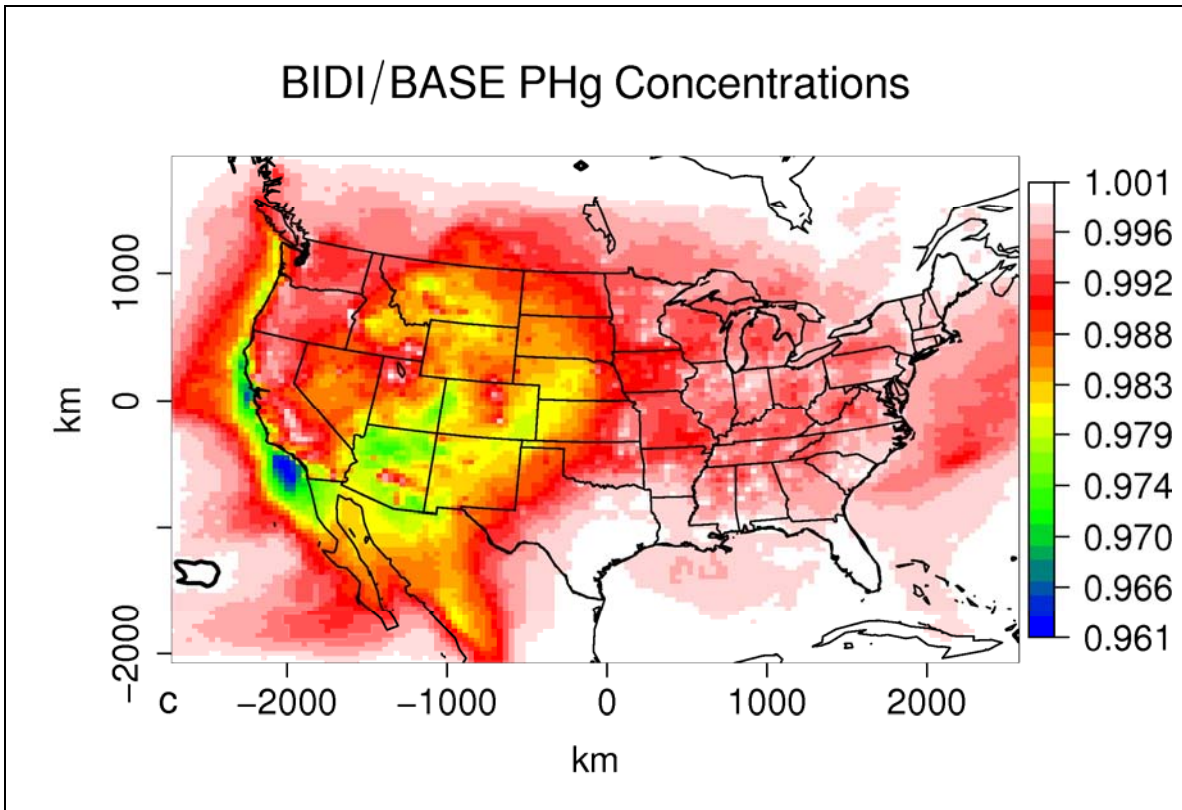
5



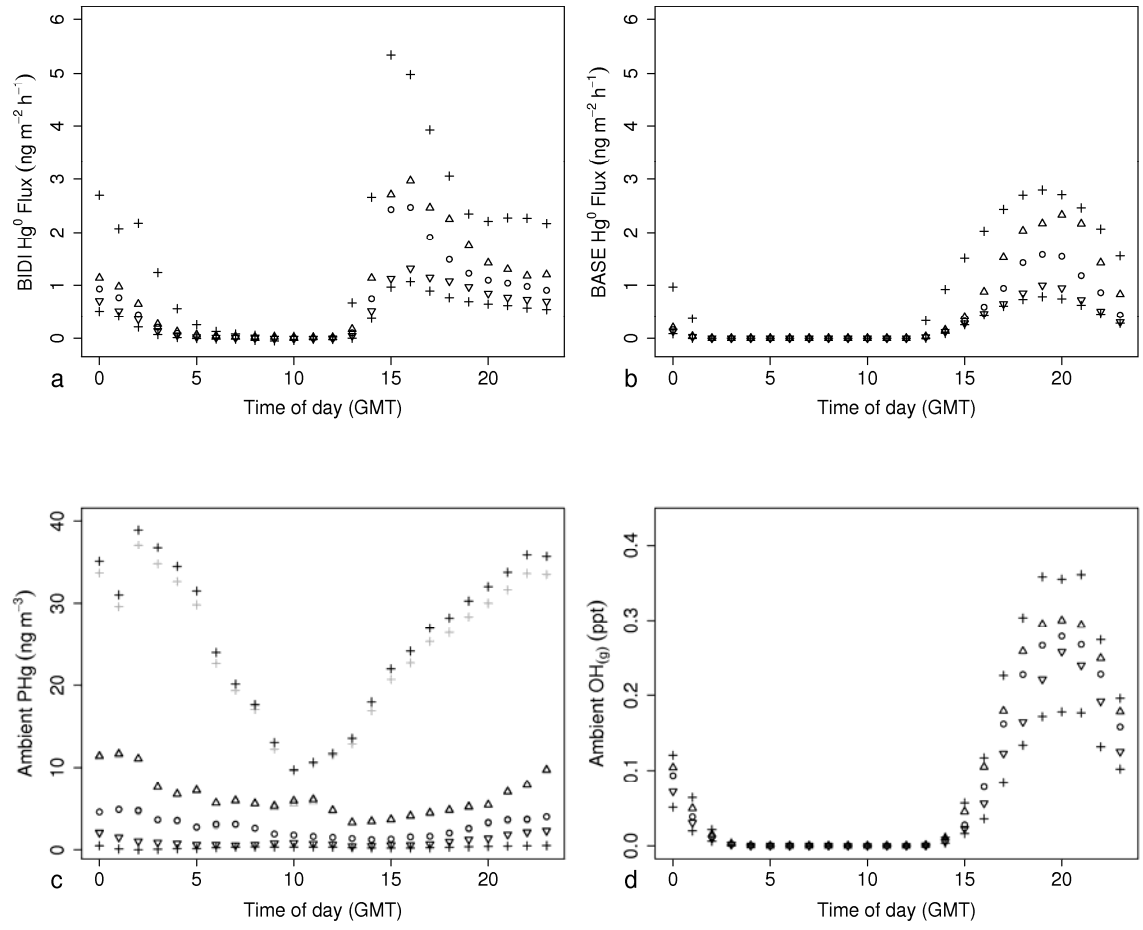
6 **Figure 5, BASE (a) and BIDI (b) median ambient layer one elemental mercury concentration**
 7 **estimates.**

8

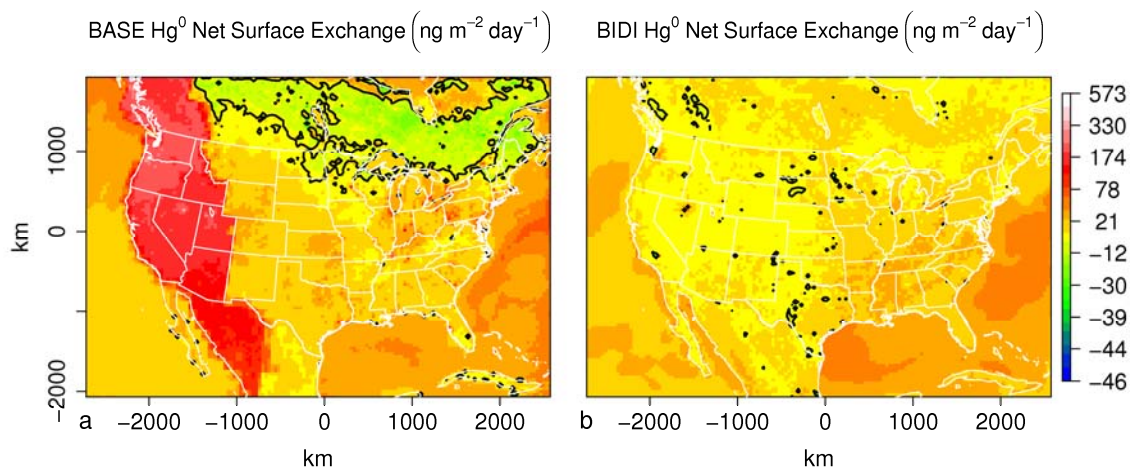




1 Figure 6, median of the ratio of the BIDI to BASE case mercury concentrations for BIDI/BASE Hg^0
 2 (a), BIDI/BASE Hg^{2+} (b) and BIDI/BASE PHg (c) from July 10th to July 31st 2002. The black contour
 3 lines denotes the area where the BIDI = BASE case concentrations.
 4

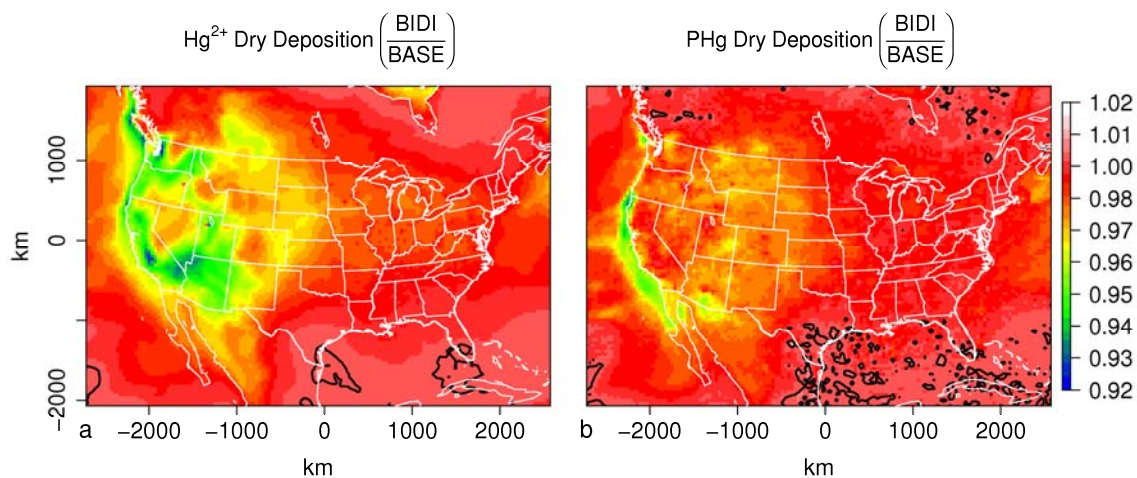


1
 2 **Figure 4, BIDI (a) and BASE (b) case Hg^0 air-sea flux, BIDI (grey) and BASE (black) PHg ambient**
 3 **concentrations (c) and OH ambient concentrations (d). The symbols are defined as: + 5th, ∇ 25th, \circ**
 4 **median, Δ 75th, and \square 95th percentiles.**
 5



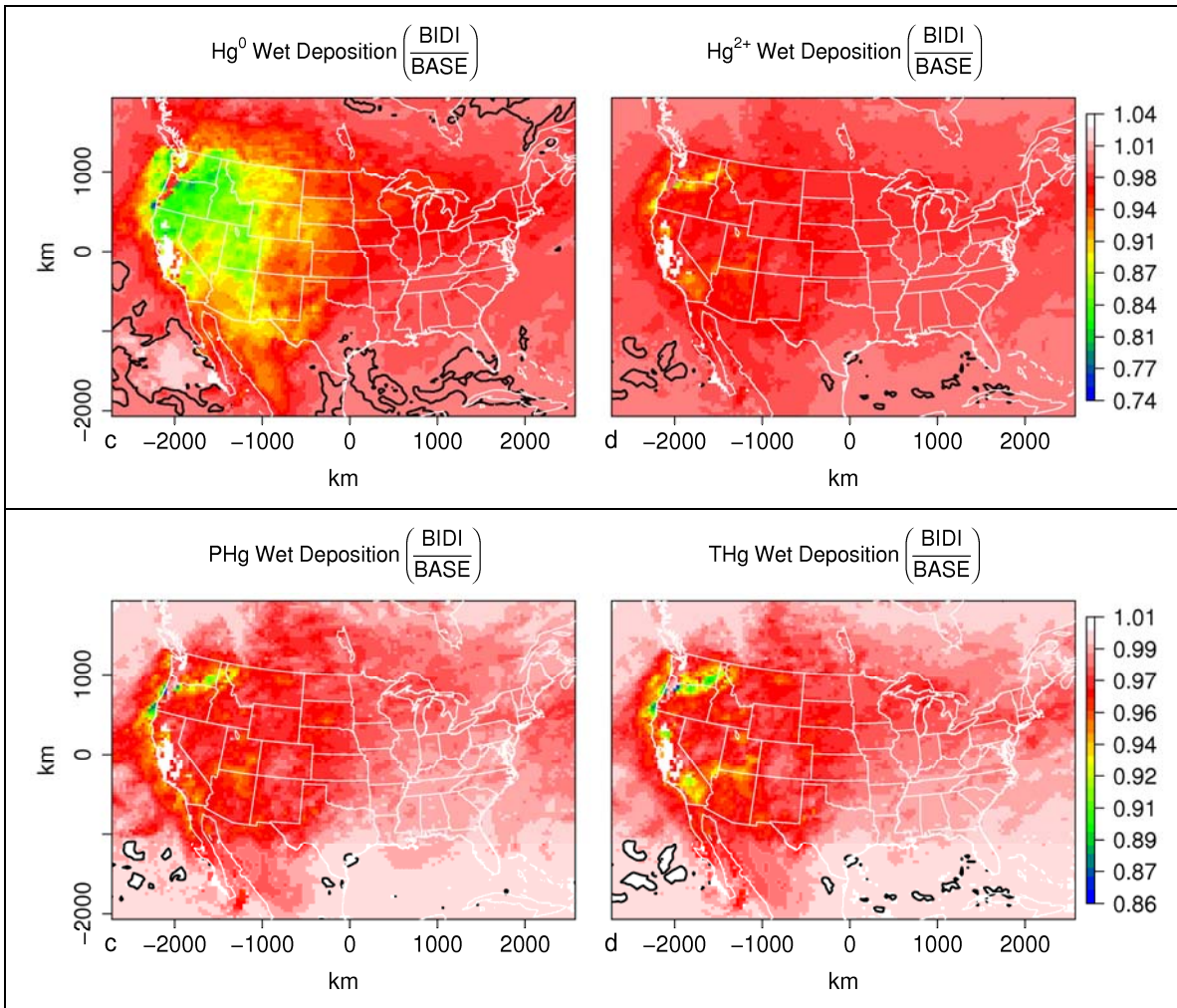
1
2
3
4
5

Figure 5, mean daily net air surface exchange of elemental mercury from July 10th through the 31st for the BASE case (a) and BIDI case (b), positive values indicate net evasion and negative values indicate net deposition, separated by the white contour line

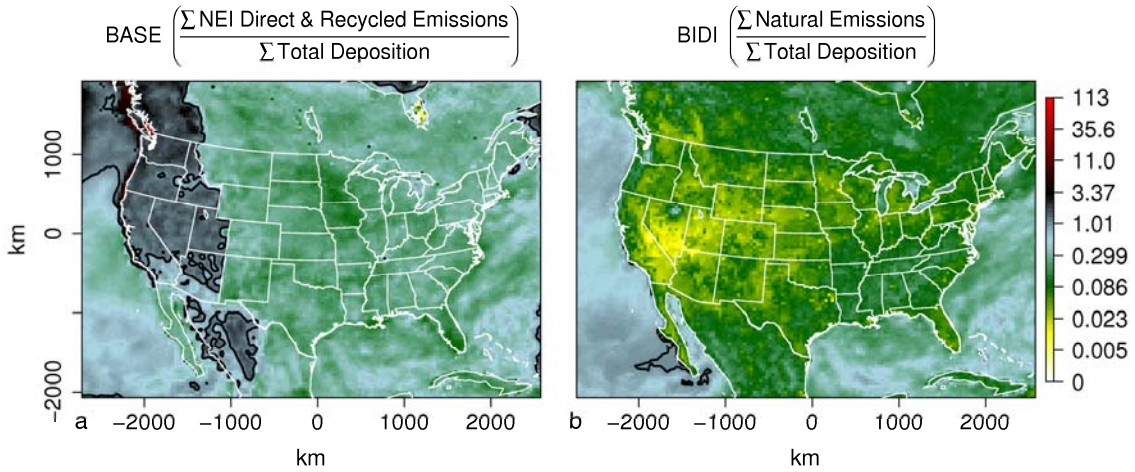


6
7
8
9
10
11

Figure 6, The mean ratio of the BIDI case to the BASE case total dry deposition of Hg^{2+} (a) and PHg (b), The black contour lines denotes the area where the BIDI = BASE case mean dry deposition.

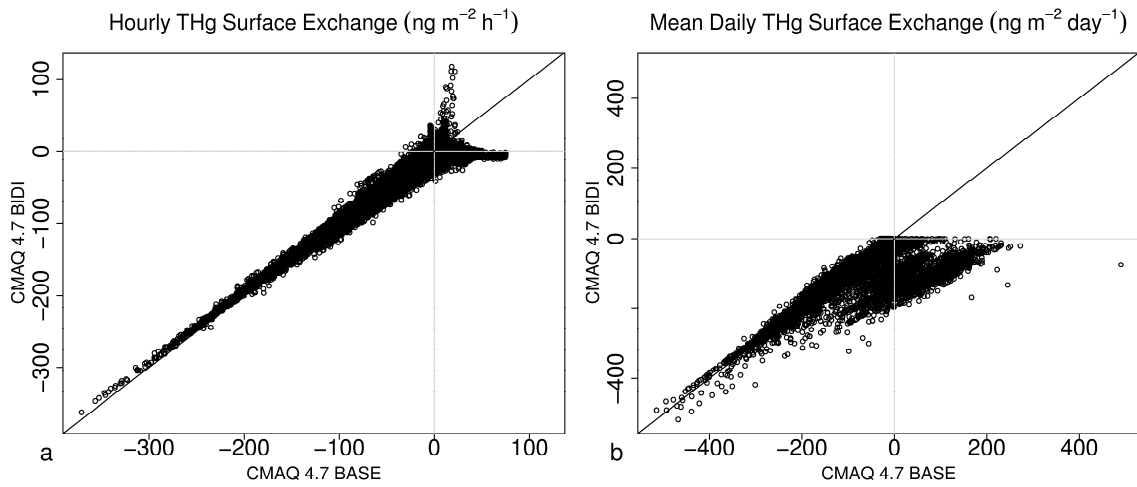


1 **Figure 7, Ratio of BIDI to BASE case wet deposition estimates of Hg^0 (a), Hg^{2+} (b), PHg (c), and total**
 2 **Hg (d) from July 10th through the 31st, black contour lines denotes the area where the BIDI = BASE**
 3 **case mean dry deposition.**
 4



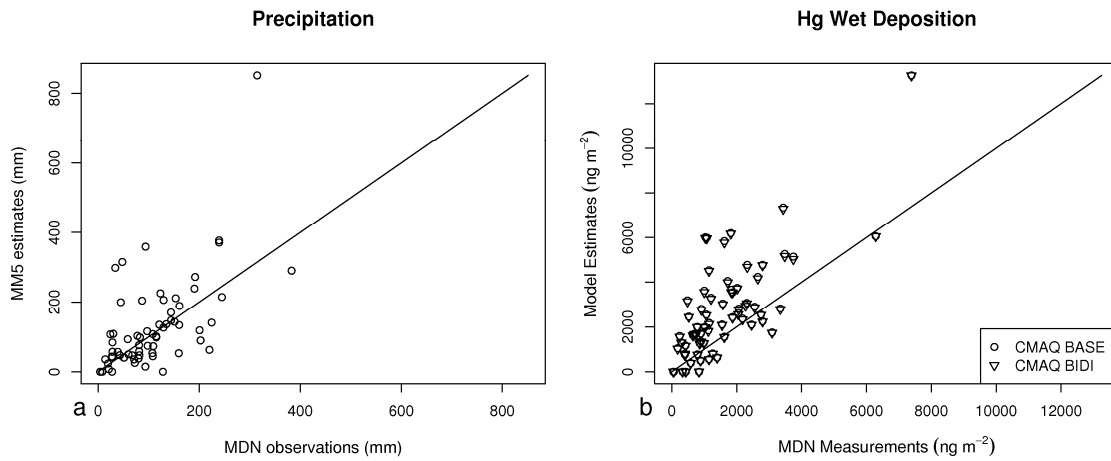
1
2
3
4
5

Figure 8, Ratio of total Hg^0 evasion from natural processes to total mercury wet and dry deposition estimated by the BASE case (a) and the BIDI case (b) from July 10th through the 31st. Black contour lines encompass areas where Hg^0 evasion exceeds the total mercury loading.



6
7
8
9
10

Figure 9, Total mercury surface exchange estimates from CMAQ 4.7 plotted against CMAQ 4.7 with bi-directional mercury exchange for hourly flux estimates (a) and the mean daily flux over the simulation period (b).



1
2
3
4
5

Figure 10, Simulated total mercury wet deposition (a) and total precipitation (b) and plotted against observed values at Mercury Deposition Network monitors for BASE (circles) and BIDI (triangles) cases.